

Genetic association study of exfoliation syndrome identifies a protective rare variant at LOXL1 and five new susceptibility loci

This is the peer reviewed version of the following article:

Original:

Aung, T., Ozaki, M., Lee, M.C., Schlotzer-Schrehardt, U., Thorleifsson, G., Mizoguchi, T., et al. (2017). Genetic association study of exfoliation syndrome identifies a protective rare variant at LOXL1 and five new susceptibility loci. NATURE GENETICS, 49(7), 993-1004 [10.1038/ng.3875].

Availability:

This version is available <http://hdl.handle.net/11365/1137336> since 2021-03-29T14:43:02Z

Published:

DOI: <http://doi.org/10.1038/ng.3875>

Terms of use:

Open Access

The terms and conditions for the reuse of this version of the manuscript are specified in the publishing policy. Works made available under a Creative Commons license can be used according to the terms and conditions of said license.

For all terms of use and more information see the publisher's website.

(Article begins on next page)



Published in final edited form as:

Nat Genet. 2017 July ; 49(7): 993–1004. doi:10.1038/ng.3875.

Genetic association study of exfoliation syndrome identifies a protective rare variant at *LOXL1* and five new susceptibility loci

A full list of authors and affiliations appears at the end of the article.

Abstract

Exfoliation syndrome (XFS) is the commonest known risk factor for secondary glaucoma and a significant cause of blindness worldwide. Variants in two genes, *LOXL1* and *CACNA1A* have been previously associated with XFS. To further elucidate the genetic basis of XFS, we collected a global sample of XFS cases to refine the association at *LOXL1*, which previously showed inconsistent results between populations, and to identify new variants associated with XFS. We identified a rare, protective allele at *LOXL1* (p.407Phe, OR = 25, $P = 2.9 \times 10^{-14}$) through deep resequencing of XFS cases and controls from 9 countries. This variant results in increased cellular adhesion strength compared to the wild-type (p.407Tyr) allele. A genome-wide association study (GWAS) of XFS cases and controls from 24 countries followed by replication in 18 countries identified seven genome-wide significant loci ($P < 5 \times 10^{-8}$). Index variants at the new loci map to chromosomes 13q12 (*POMP*), 11q23.3 (*TMEM136*), 6p21 (*AGPAT1*), 3p24 (*RBMS3*) and 5q23

Correspondence should be addressed to T. Aung (aung.tin@singhealth.com.sg), F. Pasutto (Francesca.Pasutto@uk-erlangen.de).

J.L. Wiggs (Janey_Wiggs@meei.harvard.edu), or to C.C. Khor (khorcc@gis.a-star.edu.sg).

*These authors all contributed equally to this work.

Author contributions

C.C.K., F.P., J.L.W., T.A., and M.O. jointly conceived the project.

M.C.L., U.S.-S., M.Z., D.B., Y.F.C., X.Y.N., A.W.O.C., E.N.V., S.R.G., A.S.Y.C., & Y.C. conducted functional biological experiments.

G. T., R.P.I. Jr., K.P.B., Z.L., G.P., S.S., J.N.C.B., S.U., Z.Y., L. Huang, J.N.F., R.Q.S., K.S.S., P. Kraft, I.J., A.G., M.A.P.-V., A.M.H., E.N.V., C.-Y.C., & J.L.H. conducted statistical analysis. S. Raychaudhuri provided critical input on statistical analysis.

Z.X., S.Q.M., H.M.S., X.Y.C., S.Q.P., & K.K.H. conducted genotyping and sequencing experiments.

T.A., M.O., T.M., A.H., S.E.W., Y.S.A., A.C.O., S. Nakano, K. Mori, A.P.C., K.H., S. Manabe, S. Kazama, T. Zarnowski, K.I., M. Irce, M.C.-P., K. Sugiyama, P. Schlottmann, S.F.L., H.L., Y.N., M.B., K. Ho Park, S.C.C., K.Y., J.C.Z., J.B.J., R.S.K., S.A.P., N. Kalpana, R.G., L.V., T.D., D.P.E., L.d.J.M., M.P., S. Moghimi, R.I., D.B.-H., P. Kappelgaard, B. Wiostko, S.T., D.G., K.B., W.L.G., X.C., J.S., H.J., L.J., C.Q., H.Z., X.L., B.Z., Y.-X.W., L.X., S.L., P.R., G.C., S.T., G.M., N. Weisschuh, U.H., U.-C.W.-L., C.M., P. Founti, A. Chatzikiriakidou, T.P., E.A., A.L., R.S., N.P., V.S., R.V., C. Shivkumar, N. Kobakhidze, M.R.K., A.N.B., S.Y., A.I., H.N., N. Khatibi, A.F., C.L., L.D., T.R., P. Frezzotti, D.P., E.S., P. Manunta, Y.M., K. Miyata, T.H., E.C., S.I., A.Y., M.Y., Y.K., T.O., T. Sakurai, T. Sugimoto, H.C., M.A., M. Inatani, M.M., N.G., F.M., N.Y., Y.I., M.U., C. Sotozono, J.W.J., M.S., K. Hyung Park, J.A., M.C.-A., S.M.E., A. Rafei, V.H.K.Y., M.I.K., O.O.O., A.O.A., I.U., A.O., N.K.-A., C.T., Y.S., W.S., S.O., N.U., I.A., H.A., F.A., E.K.-J., U.L., I.L., V.C., R.P.G., G.S.M., S. Roy, E.D., E. Silke, A. Rao, P. Sahay, P. Fornero, O.C., D.S., T. Zompa, R.A.M., E. Souzeau, P. Mitchell, J.J.W., A.W.H., M.C., J.G.C., S.Y.A., E.L.A., A.E., V.V., G.K., R.F., S.A.A.-O., O.O., L.A.A., B.C., R.H., S.-L.H., F.A.E.-D., R.G.-S., F.M.-T., A. Salas, K.P., L. Hansapinyo, B. Wanichwecharuang, N.K., A. Sakuntabhai, H.X.N., G.T.T.N., T.V.N., W.Z., A.B., D.S.K., M.L.H., S.D., S. Herms, S. Heegaard, M.M.N., S. Moebus, R.M.R., A.Z., T.R.C., M.R., L.A., M.G., H.G.-I., P.P.R.-C., L.F.-V.C., C.O., N.T., E.A., B.B., D.A., B.K., M.R.W., A.L.C., Y.L., P.C., L. Herndon, R.W.K., J.K., K.C., C.J.C., A. Crandall, L.M.Z., T.Y.W., M.N., S. Kinoshita, A.I.d.H., E.V., J.H.F., R.K.L., A.J.S., B.J.S., N. Wang, D.C., R.Q., T. Kivela, A. Reis, F.E.K., R.N.W., L.R.P., F.J., R.R.A., R.R., T. Kubota, S. Micheal, F.T., J.E.C., K.A.-A., M.H., J.H.K., S. Nelson, D.M., P. Sundaresan, M.D., & K.T. were involved in sample collection, phenotyping, and processing. U.T., G.T., and K. Stefansson supervised, conducted and provided analysis of deCODE data.

The manuscript was written by C.C.K., with critical input from T.A., T.K., U.T., J.L.W., L.R.P., and F.P. All co-authors approved the manuscript for publication.

Data Availability Statement

The primary dataset comprising genome-wide association summary statistics of all SNP markers reflected in the Figure 2 Manhattan plot are appended as Supplementary Dataset 2, available online. Secondary analysis datasets are appended as Supplementary Dataset 1 (*LOXL1* phased haplotype analysis) and Supplementary Dataset 3 (INRICH analysis).

Competing financial interests

The authors declare no competing financial interests.

(near *SEMA6A*). These findings provide biological insights into the pathology of XFS, and highlight a potential role for naturally occurring rare *LOXLI* variants in disease biology.

Exfoliation syndrome (XFS) is an age-related systemic disorder involving the extracellular matrix (ECM). It is characterized by the excessive production and progressive accumulation of an abnormal extracellular material in various tissues¹. Manifesting most conspicuously in the eye, XFS is the commonest cause of secondary glaucoma world-wide² and is also a prognostic factor for progression of open-angle glaucoma³. This disease is common in many populations, with an estimated 60–70 million patients affected^{4–7}. Exfoliation glaucoma (XFG) has a worse prognosis than other major types of glaucoma, and it is often resistant to intraocular pressure-lowering medical treatment, more often necessitating laser and surgical intervention^{3,8}. Cumulatively, XFS/XFG is a significant cause of blindness globally.

The strong pattern of familial aggregation for XFS indicates a significant genetic contribution to disease pathology^{9,10} and *LOXLI*, a gene coding for lysyl oxidase homolog 1, was the first genetic locus reported to be associated with this disease¹¹. Despite the overwhelming strength of the genetic association seen at polymorphisms mapping to *LOXLI*, the results are inconsistent due to risk alleles being ‘flipped’ in certain populations^{12,13}. Such stark allele reversals imply that the genetic architecture underlying XFS disease biology is complex and worthy of further study.

Recently, *CACNA1A* was identified as the second locus associated with XFS¹⁴. Realizing that large and inclusive international collaborative efforts are essential in providing new biological leads in complex disease pathogenesis^{15–20}, we report here a world-wide collaborative XFS study aimed at further understanding the genetic basis of the disorder. Firstly, due to the allele reversals seen at *LOXLI* common polymorphisms led by rs3825942 G>A (p.153Gly>Asp) and to a lesser extent, rs1048661 T>G (p.141Leu>Arg)^{12,21–28} (Supplementary Figure 1), we aimed to refine the *LOXLI* genetic landscape by performing deep sequencing of the entire gene in 5,570 XFS and XFG cases and 6,279 controls from 9 countries (Supplementary Table 1). The previously reported *CACNA1A* locus was also sequenced to assess if rare non-synonymous amino acid substitutions within the gene could provide further insights^{29–31}. In our effort to identify additional genetic variants associated with XFS, we also conduct an expanded genome-wide association study (GWAS) of 13,838 cases and 110,275 controls from countries across six continents (Supplementary Table 2, Supplementary Figures 2 and 3).

Results

A *LOXLI* rare missense variant protects against XFS.

We conducted deep re-sequencing of the entire *LOXLI* and *CACNA1A* loci (see Methods) in 5,570 XFS cases and 6,279 controls. This sequencing effort confirmed previously reported strong allele reversals at key *LOXLI* common variants and also at recently reported non-coding variants (Supplementary Tables 3, 4 and 5)^{13,21,23}.

We first analyzed the sequencing data to find unifying consistent common variants associated with XFS across ethnic groups that could have been missed by previous efforts.

Single variant analysis showed that for all common variants polymorphic across all collections studied, rs3825942 G>A (encoding for *LOXLI* p.153Gly>Asp) remains the most significantly associated variant ($P_{\text{fixed-effects}} = 4.14 \times 10^{-62}$), but with very high heterogeneity across study groups ($P_{\text{random effects}} = 0.0039$). No *LOXLI* common variant was consistently associated across all collections, and no *LOXLI* common variant surpassed genome-wide significance on random effects analysis (Supplementary Table 6). Conditioning for allele dosage at rs3825942 G>A abolished all residual evidence of association across the collections (Supplementary Table 6). The commonly reported rs1048661 T>G (p.141Leu>Arg) polymorphism was not significant in the meta-analysis of sequencing data either before ($P=0.25$) or after ($P=0.53$) conditioning for rs3825942 G>A ($P_{\text{for heterogeneity}} < 1 \times 10^{-10}$; $I^2 = 98.3\%$). Recognizing that single variant analysis could have missed a consistent *LOXLI* haplotypic association which is unreversed across populations, we followed up our search by phasing haplotypes of 57 SNPs across the entire *LOXLI* sequenced locus in 20-SNP sliding windows. All analyzed haplotypes showed reversal of effect across the locus, with no exceptions (Supplementary Dataset 1). It is thus unlikely that we may have missed an “unflipped” common variant which shows consistent association with XFS across our world-wide sample.

The re-sequencing of *LOXLI* revealed a total of 63 unique non-synonymous variants across the nine countries studied (Supplementary Table 7 and Supplementary Figure 4). Due to the limited insights shown by all the reversed *LOXLI* common haplotypes, we next evaluated the hypothesis that rare alleles collectively within *LOXLI* (MAF<1%) could contribute to XFS risk. We observed a broad enrichment of rare *LOXLI* non-synonymous variants in the normal controls compared to the XFS patients (OR = 0.46, $P = 4.2 \times 10^{-7}$; Table 1). As the vast majority of non-synonymous variants do not exert functional effects^{31–34}, we performed a second test restricting the analysis to aggregate only rare, non-synonymous variants conservatively predicted to be deleterious by all five functional effect prediction algorithms (SIFT, Polyphen 2-HumDiv, LRT score, MutationTaster, and Condel)³³. In so doing, we observed a substantially larger protective effect size conferred by rare variant burden (OR = 0.18, $P = 4.23 \times 10^{-11}$; Table 2). This protective burden of alleles conservatively predicted to affect *LOXLI* function remained significant even after accounting for co-segregation at the sentinel rs3825942 G>A SNP (Supplementary Table 8).

One of the rare, non-synonymous variants, rs201011613 A>T encoding for *LOXLI* p.407Tyr>Phe, showed genome-wide significance on single-variant analysis. This variant was conservatively predicted by all five protein functional predictive algorithms to affect *LOXLI* function, and is found exclusively in the Japanese (Table 3, Supplementary Figure 4a and 4b, Supplementary Table 7). The rare rs201011613-T (*LOXLI* p.407Phe) allele was observed in only 2 XFS cases (N= 3,909, 0.026%) but was observed in 68 out of 5,338 (0.64%) age- and hospital-matched controls (N=5,338, 0.64%) with no eye disorders (Table 3), conferring a 25-fold resistance to XFS ($P_{\text{Fisher's exact}} = 2.9 \times 10^{-14}$). We examined the individuals carrying the rare p.407Phe allele who had also undergone genome-wide genotyping for evidence of population substructure, but found no evidence that these carriers clustered along the major axes of population stratification (Supplementary Figure 5)^{35,36}.

We next examined the haplotype background for all 37 p.407Phe allele carrying Japanese individuals who underwent sequencing for the *LOXL1* locus (Table 3), and found that in 35 of the 37 individuals p.407Phe segregated with the common rs3825942-A (p.153Asp) haplotype. As previously discussed, this common rs3825942-A haplotype was associated with protection against XFS in Japan but conferred susceptibility to XFS in Black Africans and was thus only nominally significant in the meta-analysis of all collections which underwent resequencing for *LOXL1* ($P_{\text{random effects}} = 0.0039$; Supplementary Table 3).

Although the rare protective p.407Phe allele does not segregate with the common p.Arg141Leu polymorphism, functional biological testing would be needed to assess the relative impact of all three (at positions 141, 153, and 407) non-synonymous variants to LOXL1 function.

At the *CACNA1A* locus, a total of 200 unique rare, non-synonymous amino acid substitutions were observed in the coding frame of *CACNA1A* after re-sequencing in East Asians, Europeans, South Africa, and South Asians. In contrast to *LOXL1*, we did not observe any consistent evidence of association between rare variant burden at *CACNA1A* and susceptibility to exfoliation syndrome (Supplementary Table 9). This is not surprising, as only some common variant GWAS loci harbor additional rare variant burden³⁷.

Biological relevance of *LOXL1* p.Y407F.

XFS is characterized by excessive production and progressive accumulation of an abnormal fibrillar material, termed exfoliation material, containing ECM components such as elastin, fibrillin-1, and fibronectin localized to the surface of various cell types including lens epithelial cells^{1,38,39}. LOXL1 has been reported to modulate ECM biogenesis by cross-linking elastin and collagen in connective tissues^{40–42}. We thus performed experiments assaying the effects of *LOXL1* variants on ECM metabolism, with elastin, fibrillin-1, collagen type IV, and fibronectin as cellular biochemical readouts, and overall relative cell adhesion as a cellular physiological readout.

We assessed functional effects for the common, flipped p.Arg141Leu and p.Gly153Asp polymorphisms as well as the rare protective p.Tyr407Phe variant using four constructs carrying these three variants in naturally occurring haplotypes (Figure 1a). This experimental design also allowed for measurement of the effect of p.Tyr407Phe while conditioning for the effect of all p.Arg141Leu - p.Gly153Asp haplotype combinations. The ability to condition against and account for the effect of p.Gly153Asp is particularly important as the rare protective p.407Phe segregates with the p.153Asp allele. Using human lens epithelial cell (HLEC) 3D cell cultures that were transiently expressing the four haplotypes, we observed that the LOXL1 protein was secreted at detectable levels, and no significant difference in LOXL1 secretion could be observed between any of the four haplotypes (Supplementary Figure 6a).

In contrast, when we overexpressed the rare p.407Phe-carrying LOXL1–141Arg-153Asp-407Phe (G-A-T) haplotype in HLEC cultures, we observed a dose-dependent increase in elastin on Western blot (Supplementary Figure 6b), with the increase in elastin reiterated by 3D spheroid culture immunofluorescence analysis (Figure 1b).

Overexpression of this rare p.407Phe-carrying haplotype also resulted in a decrease in collagen IV (Figure 1c) and an increase in fibrillin-1 (Figure 1d) levels when compared to the other three haplotypes that included the wild-type p.407Tyr allele. This result suggests that the rare p.407Phe allele had an overall upregulating effect on ECM components such as elastin and fibrillin.

As the ECM is important for cellular adhesion, we next asked whether these observed in-vitro functional biochemical effects of the rare LOXL1 p.407Phe allele on ECM components would translate to a physiological outcome affecting cell-cell adhesion. To this end, HLEC 3D spheroids overexpressing the four haplotypes were analyzed for their relative cellular adhesion strength using the microelectrodes of the Roche xCelligence real-time cell analysis system. Using this previously described methodology, the change in cellular impedance readout is directly proportional to the quality of cell attachment^{43–45}. We observed that the rare, protective LOXL1 p.407Phe-carrying G-A-T haplotype conferred a significant increase in cellular adhesion strength in comparison to the remaining three haplotypes carrying the wild-type p.407Tyr allele ($P < 0.01$ for all comparisons; Figure 1e). We observed no significant difference in relative cellular adhesion strength when the remaining three haplotypes carrying p.407Tyr (but with different combinations of the p.Arg141Leu and p.Gly153Asp alleles) were compared to one another (Figure 1e), suggesting that the common p.Arg141Leu and p.Gly153Asp polymorphisms have no significant effect on the strength of cellular adhesion in this assay. To ensure that the increase in cell-cell adhesion was unique to the rare protective p.407Phe (rs201011613-T) allele, two additional haplotype constructs covering the G-G-T (LOXL1–141Arg-153Gly-407Phe) and T-G-T (LOXL1–141Leu-153Gly-407Phe) haplotypes were cloned. We retested all six haplotype constructs together for differences in cell-cell adhesion (Supplementary Figure 7), and continue to observe that the introduction of the rare protective p.407Phe (rs201011613-T) allele significantly increased physiological cell-cell adhesion regardless of background p.Arg141Leu and p.Gly153Asp alleles. In contrast, the haplotypes carrying the wild-type baseline p.407Tyr (rs201011613-A) allele had significantly lower cell-cell adhesion also regardless of the p.Arg141Leu and p.Gly153Asp alleles ($P < 1 \times 10^{-4}$ for all comparisons; Supplementary Figure 7).

GWAS identifies five new loci associated with XFS

As XFS is a complex disease, we also sought to identify new genetic loci associated with this disorder. For the GWAS discovery stage, we directly genotyped a total of 9,035 XFS cases and 17,008 controls enrolled from 24 countries across six continents using the Illumina OmniExpress Beadarray (Supplementary Table 2). After quality checks, we were able to analyze 683,397 directly genotyped autosomal SNP markers for association with XFS disease status (Supplementary Dataset 2)(see Supplementary Note for full details).

The GWAS discovery meta-analysis revealed consistent and significant association ($OR = 1.17$, $P = 2.97 \times 10^{-10}$, $I^2 = 0\%$; Supplementary Figure 8) at a novel locus defined by SNP rs7329408 mapping to *FLT1-POMP-SLC46A3* on chromosome 13. We also observed a clear excess of smaller-than-expected P -values at the tail end of the quantile-quantile distribution ($P = 1 \times 10^{-4}$; Supplementary Figure 8^{37,46,47}), suggesting that there are additional loci to be

identified. We forwarded all markers showing $P = 1 \times 10^{-4}$ in the GWAS discovery stage for further assessment in the replication stage (see Supplementary Table 10 for power calculations) comprising 4,803 XFS cases and 93,267 controls independently ascertained from 18 countries (Supplementary Table 2). SNPs at five distinct new loci showed consistent evidence of replication, and meta-analysis of all 13,838 cases and 110,275 controls from the GWAS and replication series revealed genome-wide significant association at the five loci (1.56×10^{-16} $P = 1.5 \times 10^{-8}$, Table 4, Figure 2, and Supplementary Figure 9; see Supplementary Table 11 for ethno-geographical stratified analysis of the five new loci). These loci are *FLT1-POMP-SLC46A3* rs7329408 (chromosome 13), *TMEM136-ARHGEF12* rs11827818 (chromosome 11) *AGPAT1* rs3130283 (chromosome 6), *RBMS3* rs12490863 (chromosome 3), and *SEMA6A* rs10072088 (chromosome 5). Regional association maps showing the genomic organization of the five loci within a 1 Mb flanking region of the sentinel SNPs are appended as Supplementary Figure 10. We verified the genotyping at the sentinel SNPs for all five loci to be of good quality (Supplementary Figure 11). We also confirm genome-wide significant association at the previously reported *CACNA1A* rs4926244 (Supplementary Table 12). Of the five new loci, only rs7329408 showed a significant latitude gradient effect, with the odds ratio of the risk allele highest in polar regions and lowest in equatorial regions (Supplementary Note and Supplementary Table 13).

Biological insights from GWAS associated loci.

We annotated 33 genes mapping to or located closest (genomic region within a 150,000bp flanking region both 5' and 3' to the sentinel SNPs and SNP markers showing $r^2 > 0.5$ with the sentinel SNPs (Supplementary Table 14), or as defined by credible set analysis^{37,48,49}, see Methods) to the seven genome-wide significant loci. Except for *AGPAT* rs3130283 which was located within the broad MHC locus on chromosome 6 which is well known for showing long range complex LD patterns, we observed that defining an 'associated locus region' either generically as ± 150 Kb from the index variant, or as the region containing proxy SNPs with $r^2 > 0.5$ with the index variant, all highlight the same genes (Supplementary Figure 10 and Supplementary Table 14). All credible sets for the 7 genome-wide significant loci were located within relatively narrow regions (<100,000 base-pairs), and within the region bound by the proxy SNPs showing $r^2 > 0.5$ with the index variant (inclusive of the index variant; Supplementary Table 14).

We next assessed the potential biological contribution for each of the 33 genes using the following criteria: 1) genes expressed in anterior segment tissues such as the iris and ciliary body from publicly available databases^{50–54}. 2) Presence of relevant eye-related phenotypes in knockout mice. 3) cis-QTL genes^{55,56}. 4) Genes prioritized by text mining in Pubmed. 5) Genes showing pleiotropy with other forms of glaucoma. 6) Highlighted genes from unbiased genome-wide molecular pathway analysis. We summarize these additional information in Supplementary Table 15. A genome-wide search using publicly available databases⁵⁷ revealed potential molecular interactions between several of the 33 genes located within the 7 genome-wide significant loci (Supplementary Table 15), suggesting that the significantly associated loci could be implicating broader yet undescribed disease biological pathways. A search of the UCSC genome browser revealed that none of the 7

genome-wide significant loci harbor any long non-coding RNA except for *LOXL1* (which harbors *LOXL1-AS1* in the opposite direction) and the *FLT1-POMP-SLC46A3* locus (Supplementary Figure 12). Further interrogation using the INRICH (interval based enrichment analysis tool) software package⁵⁸, designed for detecting enriched association signals of LD-independent genomic regions within biologically relevant gene sets did not reveal any statistically significant biological pathways highlighted by the 7 genome-wide significant loci (Supplementary Dataset 3).

We next studied the expression of genes associated with the 3 most significantly associated loci. These loci (and genes) were 13q12 (*POMP*, *FLT1*, *SLC46A3*), 11q23.3 (*TMEM136*, *ARHGEF12*), and 6p21 (*AGPAT1*). Expression for these 6 genes was tested in fresh ocular tissues obtained from human donor eyes with appropriate research consent (see Methods). For mRNA expression analyses, 41 normal eyes with no known ocular disease (mean age, 77.1 ± 8.1 years; 20 female, 21 male) and 21 eyes with XFS (mean age, 80.1 ± 7.9 years; 11 female, 10 male) were used. Messenger RNA (mRNA) expression of all 6 genes was detected at moderate levels in the panel of eye tissues analysed (Supplementary Figure 13). The highest expression levels were observed in tissues relevant for the synthesis of exfoliation material (iris, ciliary body) and for glaucoma pathophysiology (retina). Expression levels in these tissues did not significantly correlate with genotypes of the sentinel SNPs underlying the 3 loci (Supplementary Figure 14).

Comparing tissues from XFS and control eyes, mRNA expression levels of *POMP* and *TMEM136* were significantly reduced by up to 41% in anterior segment tissues of XFS eyes, such as iris and ciliary body compared to age-matched control eyes (Supplementary Figure 15). These results in XFS-relevant tissues suggest that *POMP* (rather than *FLT1* and *SLC46A3* which are located nearby) is the likely disease gene in the chromosome 13 locus and that *TMEM136* (rather than the neighbouring *ARHGEF12*) is the likely disease gene for the chromosome 11 locus.

POMP and *TMEM136* protein expression was further analysed by Western blot and immunofluorescence microscopy. *POMP*, a proteasome maturation protein, was shown to be expressed in most ocular cell types by immunofluorescence (Figure 3). However, *POMP* protein expression was significantly reduced in iris (–45%) and ciliary body (–33%) specimens from XFS eyes compared to control eyes when investigated using Western blots (Figure 3G and Supplementary Figure 16) and using immunofluorescence microscopy (Figures 3H, 3J, and 3K, and Figures 3L, 3M, and 3N). These results are consistent with the differential mRNA expression shown in Supplementary Figure 15.

TMEM136, a transmembrane protein of unknown function, was primarily immunolocalized to vascular endothelial cells of blood vessels in eye tissues (Figure 4). Analysis of *TMEM136* protein expression by Western blot and tissue from eyes with XFS showed significantly reduced expression levels in iris (–26%) and ciliary body (–32%) (Figure 4G and Supplementary Figure 17) compared to that observed in control eyes, also consistent with the differential mRNA expression analysis shown in Supplementary Figure 15. Similar findings showing reduced *TMEM136* protein staining in epithelial and endothelial cells in

XFS eyes compared to controls eyes were also observed using immunofluorescence microscopy (Figures 4H, 4J, 4K, and Figures 4L, 4M, and 4N).

We then replicated the immunofluorescence microscopy findings in tissues from a further 3 donor eyes with XFS and 3 matched controls using an independent batch of antibodies, co-staining for LOXL1, POMP, and TMEM136. We confirmed reduced expression of POMP and TMEM136 in important ocular anterior segment structures in XFS eyes compared to controls, on both low magnification (Supplementary Figure 18) and higher magnification (Supplementary Figures 19 and 20).

Discussion

XFS is a disorder of aging involving the ECM, with LOXL1 hypothesized to play a central role in disease pathogenesis. As all common *LOXL1* haplotypes detected by the resequencing effort showed reversal of genetic effect, their functional consequences remain in doubt. Even a recent study describing a region in intron 1 of *LOXL1* and 5' upstream of *LOXL1-AS1* containing a promoter that influences *LOXL1-AS1* expression showed that all strongly associated variants influencing the promoter activity of *LOXL1-AS1* also have genome-wide significant reversal of genetic effect²¹. The common allele reversals at *LOXL1* are unlikely to be due to sampling differences within the same population in light of multiple replications confirming the reversal. It is also unlikely to be due to different LD structures across different populations due to the reversal occurring across all phased haplotypes along the broad *LOXL1* locus (Supplementary Dataset 1) in the absence of gross differences in LD architecture (Supplementary Figure 21).

Deep resequencing of *LOXL1* enabled us to observe that the rare p.Tyr407Phe variant had a protective effect strong enough ($OR_{\text{for resistance}}=25$) to surpass genome-wide significance on its own. Although strong, the protection is not absolute, as the variant was observed in 2 XFS patients. Both patients also carry a copy of the *TMEM136* rs11827818-G risk allele, in keeping with XFS being a complex disease. Our experiments confirm a clear functional and physiological role for the rare p.407Phe allele, but less so for the common p.153Gly>Asp and p.141Leu>Arg polymorphisms.

The protective p.Tyr407Phe substitution is located in the evolutionarily conserved catalytic domain of LOXL1⁵⁹. Follow up biological experiments suggests that the protective effect may be a consequence of stabilization of the ECM due to increased elastin and fibrillin-1 deposition. This notion is supported by histopathological observations demonstrating decreased elastic fiber formation and tissue stiffness as well as impaired cell adhesion in ocular tissues of patients with XFS^{60,61}. We speculate that carrying the rare protective p.407Tyr variant could maintain cellular integrity and render cells more resistant to environmental stressors which destabilize or disrupt the ECM. One limitation of this approach is that the biological mechanisms for p.Tyr407Phe were not tested at the RNA level, as there is a possibility that p.Tyr407Phe could affect RNA stability^{62–64}.

The seven loci emerging from the GWAS study do not implicate a single pathogenesis pathway, supporting the hypothesis that XFS is a complex systemic disease of aging that can

arise from genetic lesions in multiple pathways and different tissue types. For example, the marked downregulation of POMP (Figure 3), a ubiquitously expressed proteasome maturation protein in XFS tissues suggests a reduction of ubiquitin conjugating enzymes in XFS tissues⁶⁵. Abnormalities in the closely related autophagy pathway have also been implicated in XFS⁶⁶, a process that also involves ubiquitin-proteasome signaling^{67,68}. TMEM136 expression was predominantly localized to vascular endothelia. Interestingly, a pronounced and early vasculopathy, partly involving XFS material deposits around ocular blood vessels (Figure 4) appears to play a significant role in XFS pathophysiology^{69,70}.

In addition to *POMP* and *TMEM136*, in this study we also identified 3 other XFS susceptibility loci that map to: *AGPAT1* in the class III MHC region (6p21), to *RBMS3* (3p24), and near *SEMA6A* (5q23). *AGPAT1* has been identified as a susceptibility locus for Omega6 (n6) polyunsaturated fatty acids (PUFAs) levels in the CHARGE consortium, which may be related to cardiovascular risk in aging populations⁷¹. The MHC locus (where *AGPAT1* resides) has also been reported to be involved in conditions such as Alzheimer's and Parkinson's disease^{72,73}, which, like XFS, are age-related conditions. Although the biological roles of *AGPAT1*, *RBMS3* and *SEMA6A* are not well understood, the consistent evidence of association at these loci thus opens up further avenues for research into XFS disease biology.

In summary we now show that a rare *LOXLI* variant, p.Tyr407Phe, strongly protects against XFS, raising the possibility of potential pharmacological targeting of LOXL1 for therapeutic purposes^{29,74–76}. In addition, we have identified 5 new XFS loci that implicate new biological pathways which could be important for disease pathogenesis.

Online methods

Patient collections

DNA and tissue samples from all patients with XFS and exfoliation glaucoma together with normal controls without XFS were obtained after informed written consent from each participant. All human samples were obtained in strict adherence to the tenets of the Declaration of Helsinki. Details for each XFS case control collection are appended in Supplementary Note.

Genotyping of samples

For the GWAS discovery stage performed in 24 countries (considered across 25 strata due to Russia contributing two distinct collections, one from St Petersburg and one from the Republic of Bashkortostan; Supplementary Table 2), genome-wide genotyping was undertaken using the Illumina OmniExpress Beadchip, as previously described¹⁴. To minimize bias between different genotyping arrays and platforms, all 9,035 XFS cases and 17,008 controls for the GWAS discovery stage were genotyped using the Illumina OmniExpress array, ensuring that the primary discovery analysis used only directly genotyped SNP markers uniformly genotyped in cases and controls. The absence of imputation on primary discovery analysis means that issues due to imputation uncertainty

and insufficient information content for imputed SNPs with varying minor allele frequencies across the different ethnic groups is minimized⁷⁷.

The replication stage included XFS collections from 18 countries (Supplementary Table 2). Details on the genotyping and analysis for the replication stage are appended in Supplementary Note.

Statistical analysis for the GWAS discovery stage

Stringent quality control checks were performed for each SNP marker and each individual sample. Our statistical analysis protocol for the GWAS discovery stage only included directly genotyped SNP markers genotyped by the Illumina OmniExpress bead array. We removed poorly performing SNP markers showing genotyping completion rates of <95%, as well as SNPs showing significant deviation from Hardy-Weinberg equilibrium ($P < 1 \times 10^{-6}$ for deviation). SNPs with minor allele frequency of <1% were also removed from further GWAS discovery analysis. Each sample was similarly checked, and those with poor genotyping success rate (defined as genotyping completeness < 95%), showing excess heterozygosity defined as > 3 standard deviations from the mean^{78,79}, and have outlying genetic ancestry (defined by more than six standard deviations from the mean on principal component analysis⁸⁰) were excluded from further analysis.

We verified the biological relationships of all samples remaining after further exclusion of samples using the principle of variability in allele sharing. We used the PLINK software (See URLs) to derive information for identify-by-state status for each sample pair comparison. For each sample pair showing evidence of cryptic relatedness (IBD > 0.1875)⁷⁸, the sample with the lower genotyping completeness rate was removed from further analysis.

We performed principal component analysis to assess the degree of genetic stratification and population substructure for all samples which underwent genome-wide genotyping, as previously described⁸⁰. Principal component analysis was performed for each country / site separately to remove samples with outlying ancestry from further analysis. Principal component scores were then calculated from a pruned set of unlinked markers (defined as pair-wise $r^2 < 0.1$) for each country / site separately. These scores were used as covariates to adjust for residual population stratification. Principal component plots were executed using the R statistical program package (See URLs).

Association between SNP genotypes and XFS disease status was measured using logistic regression for each separate country strata before meta-analysis was conducted, as described elsewhere^{15,81,82}. For the GWAS discovery stage, association analysis was additionally adjusted for the first three principal components of genetic stratification for sample collections to minimize residual population stratification. The genome-wide association summary statistics of all SNP markers from the GWAS are appended as Supplementary

URLs

PLINK software, <http://pngu.mgh.harvard.edu/~purcell/plink/>; R statistical program package, <https://www.r-project.org/>; IMPUTE2 software, https://mathgen.stats.ox.ac.uk/impute/impute_v2.html; Power calculator for genetic association studies, <http://pngu.mgh.harvard.edu/~purcell/gpc/>; Primer3 software, <http://primer3.ut.ee>.

Dataset 2, available online. The genomic inflation estimate (λ_{gc}) was calculated using directly genotyped SNPs only, using the median regression test statistic, which is distributed in a chi-square manner⁸³. λ_{gc} is listed for each individual GWAS discovery strata (and also pictured in Supplementary Figure 22) as well as for the GWAS meta-analysis (Supplementary Table 2). In line with well-described methodologies, results for the seven genome-wide significant loci have undergone double gc correction which corrects for genomic inflation first at the individual population strata and then once again during meta-analysis^{84,85}.

Meta-analysis was performed via the inverse-variance, fixed effects model using genomic control corrected summary results (adjusted odds ratios and standard errors) from each separate country/site. At no point in the analysis were samples pooled within or across continental groups for association analysis, as this measure does not appropriately account for population stratification. The meta-analysis method validates strong reversal at *LOXL1* (Supplementary Figure 23).

Statistical analysis for the replication stage.

SNPs showing association with XFS surpassing $P = 1 \times 10^{-4}$ in the GWAS discovery stage were brought forward to the replication stage, and analyzed in a manner similar to that performed for the discovery stage (Supplementary Note).

Genotype imputation

For the five newly identified genome-wide significant loci, we sought to improve on genetic resolution provided by the directly genotyped SNPs currently included on standard content GWAS arrays via imputation fine-mapping using samples and SNP markers passing strict quality control checks. This would also allow for better delineation of the credible sets underlying each of the five newly identified loci⁴⁸. The imputation and phasing of genotypes were carried out using the IMPUTE2 software (See URLs) with reference panel constructed from cosmopolitan population haplotypes based on data obtained from 2535 individuals from 26 distinct populations around the world. This data is part of the 1000 Genomes project Phase 3 (Jun 2014) release, as described elsewhere. To minimize the effect of imputation uncertainty, we only included imputed genotypes with an information score of > 0.95 . Allele dosages were used for the imputed data association analyses with the software SNPTEST in order to average across imputation uncertainty.

Credible set analysis

Credible sets of SNPs were defined, as previously described, as the minimum number of genetic variants which account for $> 95\%$ probability of driving each locus-specific association signal^{48,49}. For the construction of credible sets, we included all genotyped variants with genotyping success rates of $> 95\%$ percent and minor allele frequency $> 1\%$ percent. Fine-mapping imputation variants were included using similar thresholds of minor allele frequency $> 1\%$ percent and imputation information content > 0.95 to reduce the impact of imputation quality on the credible set analysis. For the fine-mapping imputation step, allele dosages were used for the imputed data association analyses with the software SNPTEST in order to average across imputation uncertainty.

Statistical test for interaction with geographical latitude

Statistical tests for interaction between genetic markers and geographical latitude were undertaken for the five newly identified loci showing genome-wide significant association with XFS. The odds ratios and standard error for the odds ratio estimate for each SNP to be tested are assigned a latitude band for the country (or zone, whichever is more precise) where XFS cases and controls were drawn from (see Supplementary Table 2).

The odds ratios and standard error used in this test have already undergone PCA adjustment and genomic control correction during the GWAS analysis. We then conduct a trend test to assess whether the odds ratios for disease increases with increasing 10-degree increments of geographical latitude.

Mouse model phenotypes

For the 33 genes implicated by the 7 genome-wide significant SNPs on 7 distinct loci (Supplementary Table 15), we looked up the Mouse Genome Informatics publicly available database⁸⁶. The output is manually checked and curated, with the relevant references detailing the mouse models appended as footnotes in Supplementary Table 15.

Deep sequencing of *LOXL1* and *CACNA1A*

Deep sequencing was performed on a total of 5,570 XFS cases and 6,279 controls from 9 countries (Supplementary Table 1). Both the *LOXL1* and *CACNA1A* genetic loci (exons, introns, 5' and 3' flanking regions) spanning coordinates chr15:74,200,000 to 74,260,000 and Chr19:13,307,000 to 13,745,000 were captured using the Roche Nimblegen SeqCap Easy probe kit. Enrichment and amplification of the libraries were then created using well-described, routine laboratory techniques³⁶. Sequencing was performed using 2×101 paired end reads using the Illumina Hi-Seq 2500 platform. We required that >95% of the samples to be covered at least 10X⁸⁷. Mean coverage for sequencing across the samples was observed to be 60X.

For the analysis of *LOXL1* p.Y407F, the initial 2,827 cases and 3,013 controls from Japan which underwent re-sequencing were enrolled from December 2007 to January 2015. A further 1,082 exfoliation syndrome cases and 2,325 controls from Japan were enrolled for the replication stage. These samples were collected between February 2015 and December 2016 and did not undergo deep sequencing of the entire *LOXL1* locus.

Read-mapping, variant detection and annotation.

All sequence reads in each individual were aligned to the human reference genome (hg19) using the Burrows-Wheeler Aligner software, which is well described³⁶. Consensus genotypes were called using the GATK best practices guidelines. Only high quality variants assigned 'PASS' scores by variant quality score recalibration and individuals with variant genotype calling completeness >95% were brought forward for further statistical analysis.

Power calculations for genetic association study

Power calculations for the GWAS discovery and replication stages were performed on an additive genetic model using well described methods (See URLs), and is shown in

Supplementary Table 10. These power calculations take into account the asymmetric number of cases and controls, as is well reported in genetic association studies^{82,88}.

Haplotype phasing for the *LOXL1* locus

To ensure accurate phasing in order to reliably capture both common and rare haplotypes, we only included individuals with a genotype call completeness rate of 100% from both the sequencing and GWAS experiments. *LOXL1* haplotypes were phased using the BEAGLE⁸⁹ and PLINK⁹⁰ software packages, as previously described³⁵.

Tissue specimens for analysis of the GWAS loci.

Human donor eyes used for corneal transplantation with appropriate research consent were obtained and processed within 15 hours after death. For RNA and DNA extractions, 21 donor eyes with XFS (mean age, 80.1 ± 7.9 years; 11 female, 10 male) and 41 normal, healthy, age-matched control eyes (mean age, 77.1 ± 8.1 years; 20 female, 21 male) without any known ocular disease were used. Ocular tissues were prepared under a dissecting microscope and were snap frozen in liquid nitrogen. The presence of characteristic exfoliation material deposits was assessed by macroscopic inspection of anterior segment structures and confirmed by electron microscopic analysis of small tissue sectors.

For immunostaining experiments, ocular tissue samples obtained from 10 donor eyes with XFS (mean age, 78.7 ± 9.7 years; 6 female, 4 male) and 10 normal human donor eyes (mean age, 72.3 ± 11.6 years; 5 female, 5 male) were embedded in optimal cutting temperature compound and frozen in liquid nitrogen. DNA samples obtained from ocular tissues and cells were genotyped by Sanger sequencing (Supplementary Note).

Real-time PCR of human eye tissues

Ocular tissues were extracted using the Precellys 24 homogenizer and lysing kit together with the AllPrep DNA/RNA kit (Qiagen, Hilden, Germany) according to the manufacturer's instructions. This includes an on-column DNase I digestion step. First-strand cDNA synthesis from 0.5 µg of total RNA was performed with Superscript II reverse transcriptase (Invitrogen, Karlsruhe, Germany) in a 20 µl reaction volume. Quantitative real-time PCR was performed using the CFX Connect thermal cycler and software (Bio-Rad Laboratories, München, Germany). PCR reactions (25 µl) were run in duplicate and contained 2 µl of first-strand cDNA, 0.4 µM each of upstream- and downstream-primer, and SsoFast EvaGreen Supermix (Bio-Rad). Exon-spanning primers (Eurofins Genomics, Ebersberg, Germany), designed using Primer 3 software (See URLs), and PCR conditions are appended in Supplementary Table 16. For normalization of gene expression levels, mRNA ratios relative to the house-keeping gene GAPDH were calculated by the comparative C_T method (2^{-C_T}). Amplification specificity was checked using melt curve and sequence analyses using the Prism 3100 DNA-sequencer (Applied Biosystems, Foster City, CA).

Western blot analysis of human eye tissues

Total protein was extracted from iris and ciliary body tissues of 6 eyes with XFS and 6 normal eyes using RIPA buffer (50 mM Tris-HCl, pH 8.0, 150 mM NaCl, 1% NP-40, 0.5% DOC, 0.1% SDS). Protein concentrations were determined by the Micro-BCA protein assay

kit (Thermo Scientific). Proteins (10 µg per lane) were separated by 4–15% SDS-polyacrylamide gel electrophoresis under reducing conditions (6% DTT) and transferred onto nitrocellulose membranes with the Trans-Blot Turbo transfer system (Bio-Rad). Membranes were blocked with SuperBlock T20 (Thermo Scientific) for 30 minutes and incubated for 1h at room temperature or overnight at 4°C with antibodies against POMP (Abcam) and TMEM136 (Abcam) diluted in PBST/10% SuperBlock T20. Equal loading was verified with mouse anti-human p- actin antibody (clone AC-15; Sigma-Aldrich) in PBST/10% SuperBlock T20. In negative control experiments, the primary antibody was replaced by PBST. Immunodetection was performed with a horseradish peroxidase-conjugated secondary antibody in PBST/10% SuperBlock T20 and the Super Signal West Femto ECL kit (Thermo Scientific), and band intensity was analysed by computerized densitometry.

Immunohistochemistry of human eye tissues follow routine laboratory procedures, and are appended in Supplementary Note.

LOXL1 constructs

The full-length cDNA encoding LOXL1 was amplified using the primers shown in Supplementary Table 16. The restriction enzymes sites, EcoRI and Sa/I were added in a second amplification using a second set of primers (Supplementary Table 17). The LOXL1 fragment (~1.7kb) was then subcloned into a HA- tagged pcipuro vector. Four haplotypes LOXL1-Arg141-Gly153-Tyr407 (G-G-A), LOXL1-Leu141-Gly153- Tyr407 (T-G-A), LOXL1-Arg141-Asp153-Tyr407 (G-A-A), and LOXL1-Arg141-Asp153-Phe407 (G-A-T) were generated and contained genetic variants in the following order; rs1048661 (G>T)-rs3825942 (G>A)-rs201011613 (A>T). The first haplotype generated was LOXL1-Arg141-Asp153-Tyr407 (G-A-A) and it served as the template plasmid for subsequent site-directed mutagenesis.

Targeted base-substitution was generated by site-directed mutagenesis using a PCR-based strategy with Transformer™ site-directed mutagenesis kit (Clontech) with respective oligonucleotide primer pairs (Supplementary Table 17) onto the LOXL1-Arg141-Asp153-Tyr407 (G-A-A) haplotype. All accuracy of haplotypes constructed were confirmed by Sanger sequencing of the full length clone. All oligonucleotide primer pairs used to create the LOXL1 constructs are appended in Supplementary Table 17.

Nano luciferase secretion assay for LOXL1

The secretion assay for LOXL1 with respect to the four tested haplotypes LOXL1-Arg141-Gly153-Tyr407 (G-G-A), LOXL1-Leu141-Gly153-Tyr407 (T-G-A), LOXL1-Arg141-Asp153-Tyr407 (G-A-A), and LOXL1- Arg141-Asp153-Phe407 (G-A-T) were measured using the NanoLuc luciferase assay. More details for this assay are appended in Supplementary Note.

Details for Western blot analysis of the different hemagglutinin-tagged LOXL1 haplotypes on elastin, fibronectin, and collagen IV follow routine laboratory procedures, and are appended in Supplementary Note.

Spheroid cultures

The human lens epithelial cell line (HLEC (B-3)) was obtained from the American Tissue Culture Collection (ATCC). The cells were maintained in Dulbecco's modified Eagle's medium supplemented with 20% fetal bovine serum (Sigma-Aldrich) and 2mM Glutamax (Invitrogen) at 37°C with 5% CO₂, and passaged every 2–3 days in a 1:4 ratio. The cell line was tested for mycoplasma and was found to be negative.

Nucleofected HLECs were trypsinized 48 hours post-nucleofection and seeded in their growth media in low attachment 6-well plates with hydrophobic surfaces (Greiner Bio-One GmbH) at 300,000 cells per well. Cells were left to form spheroids and collected at 72 hours. The spheroids were fixed with 4% paraformaldehyde for 10min at room temperature and stored at 4°C. Fixed spheroids were washed with PBST (0.1% Tween-20 in 1× PBS) and blocked in blocking buffer (3% BSA in PBS) for 1 hour at room temperature. They were subsequently incubated overnight at 4°C with the following primary antibodies: mouse or rabbit antibody to HA (1:100 dilution; sc-7392; sc-805; Santa Cruz), goat antibody to elastin (1:100 dilution; sc-17581; Santa Cruz), mouse antibody to fibrillin-1 (1:100 dilution; ab6328; Abcam), and rabbit antibody to collagen IV (1:100 dilution; ab6586; Abcam). All antibodies were diluted with the blocking buffer. After incubation with the primary antibody, the spheroids were washed three times with PBST and labeled with their respective secondary antibodies for 1 hour at room temperature. Secondary antibodies used were with FITC, Cy3 or AlexaFluor 647-conjugated anti-mouse, anti-rabbit, or anti-goat secondary antibody (1:300 dilution; Jackson Laboratories). The spheroids were stained with DAPI (1µg/mL) and mounted on microscope glass slides using a cytocentrifuge (Thermo Fisher Scientific Inc.) and FluorSave Reagent (Merck Millipore). Immunolabelled spheroids images were acquired at the Advanced Bioimaging Core at the Academia, Singapore Health Services with a Leica TCS SP8 confocal laser scanning platform, Z-planes were imaged in 1µm steps. Analysis of spheroids was done on a maximal projection image of 5 Z-planes onto a single image. Heat map of respective immunofluorescent signals were generated relative to the minimum and maximum fluorescence intensity values of the same scale defined by the color range as indicated within the figures. Each experiment was repeated independently three times, with images also acquired independently three times.

Cell-cell adhesion assay

HLECs nucleofected with LOXL1-Arg141-Gly153-Tyr407 (G-G-A), LOXL1-Leu141-Gly153-Tyr407 (T-G- A), LOXL1-Arg141-Asp153-Tyr407 (G-A-A), and LOXL1-Arg141-Asp153-Phe407 (G-A-T) haplotype constructs were plated into 96-well plates designed for the xCELLigence RTCA SP instrument (ACEA Biosciences Inc) at a density of 120,000 cells per well. The 96-well plates were incubated at 37°C with 5% CO₂ and monitored on the xCELLigence RTCA SP system at 15-min intervals for the first 24 h and at 30-min intervals for the subsequent 48 h. The impedance data was extracted from the RTCA software and analyzed for differences in cell-cell adhesion between the different LOXL1 haplotypes. Triplicates were performed for HLECs nucleofected with each haplotype to allow for robust statistical evaluation of the results obtained. The readings for each variant were normalized against their respective initial readings at the first time point, and the normalized readings were subsequently compared against the LOXL1-Arg141-Asp153-

Phe407 (G-A-T) haplotype. The assay shown in Figure 1e was repeated four independent times, with the follow up independent experiment (shown in Supplementary Figure 7) repeated seven independent times.

Statistical procedures for biological analysis.

Statistical evaluation of expression differences between patients and controls was performed using SPSS v.20 software (IBM, Ehningen, Germany) with an unpaired two-tailed t test. $P < 0.05$ was considered statistically significant. Data for adhesion and secretion assays were analyzed by an unpaired homoscedastic t test, and two-tailed P -values were calculated. We considered $P < 0.05$ as statistically significant.

Supplementary Material

Refer to Web version on PubMed Central for supplementary material.

Authors

Tin Aung^{1,2,3,*}, Mineo Ozaki^{4,5,*}, Mei Chin Lee^{1,6,*}, Ursula Schlötzer-Schrehardt^{7,*}, Gudmar Thorleifsson^{8,*}, Takanori Mizoguchi^{9,*}, Robert P. Igo Jr.^{10,*}, Aravind Haripriya^{11,*}, Susan E Williams^{12,*}, Yury S. Astakhov^{13,*}, Andrew C Orr^{14,15,*}, Kathryn P. Burdon^{16,17,*}, Satoko Nakano^{18,*}, Kazuhiko Mori^{19,*}, Khaled Abu-Amero^{20,21,*}, Michael Hauser^{1,22,23,*}, Zheng Li²⁴, Gopalakrishnan Prakadeeswari²⁵, Jessica N. Cooke Bailey¹⁰, Alina Popa Cherecheanu^{26,27}, Jae H Kang²⁸, Sarah Nelson²⁹, Ken Hayashi³⁰, Shin-ichi Manabe³⁰, Shigeyasu Kazama³¹, Tomasz Zarnowski³², Kenji Inoue³³, Murat Irkeç³⁴, Miguel Coca-Prados^{35,36,37}, Kazuhisa Sugiyama³⁸, Irma Järvelä³⁹, Patricio Schlottmann⁴⁰, S. Fabian Lerner⁴¹, Hasnaa Lamari⁴², Yildirim Nilgün⁴³, Mukharram Bikbov⁴⁴, Ki Ho Park⁴⁵, Soon Cheol Cha⁴⁶, Kenji Yamashiro^{47,48}, Juan C. Zenteno^{49,50}, Jost B. Jonas^{51,52}, Rajesh S Kumar⁵³, Shamira A Perera^{1,2}, Anita S.Y. Chan^{1,2,6}, Nino Kobakhidze⁵⁴, Ronnie George⁵⁵, Lingam Vijaya⁵⁵, Tan Do⁵⁶, Deepak P. Edward^{57,58}, Lourdes de Juan Marcos^{59,60}, Mohammad Pakravan⁶¹, Sasan Moghimi⁶², Ryuichi Ideta⁶³, Daniella Bach-Holm⁶⁴, Per Kappelgaard⁶⁴, Barbara Wirostko⁶⁵, Samuel Thomas⁶⁵, Daniel Gaston¹⁵, Karen Bedard¹⁵, Wenda L Greer¹⁵, Zhenglin Yang^{66,67}, Xueyi Chen⁶⁸, Lulin Huang^{69,70}, Jinghong Sang⁷¹, Hongyan Jia⁷¹, Liyun Jia^{52,71}, Chunyan Qiao⁷¹, Hui Zhang⁷¹, Xuyang Liu⁷², Bowen Zhao^{52,71}, Ya-Xing Wang⁵², Liang Xu⁷¹, Stéphanie Leruez⁷³, Pascal Reynier⁷⁴, George Chichua⁵⁴, Sergo Tabagari⁷⁵, Steffen Uebe⁷⁶, Matthias Zenkel⁷, Daniel Berner⁷, Georg Mossböck⁷⁷, Nicole Weisschuh⁷⁸, Ursula Hoja⁷, Ulrich-Christoph Welge-Luessen⁷, Christian Mardin⁷, Panayiota Founti⁷⁹, Anthi Chatzikyriakidou⁸⁰, Theofanis Pappas⁷⁹, Eleftherios Anastasopoulos⁷⁹, Alexandros Lambropoulos⁸⁰, Arkasubhra Ghosh⁸¹, Rohit Shetty⁸², Natalia Porporato⁸³, Vijayan Saravanan²⁵, Rengaraj Venkatesh⁸⁴, Chandrashekarani Shivkumar⁸⁵, Narendran Kalpana⁸⁶, Sripriya Sarangapani⁸⁷, Mozhgan R Kanavi⁸⁸, Afsaneh Naderi Beni⁶¹, Shahin Yazdani⁶¹, Alireza Iashay⁶², Homa Naderifar⁶², Nassim Khatibi⁶², Antonio Fea⁸⁹, Carlo Lavia⁸⁹, Laura Dallorto⁸⁹, Teresa Rolle⁸⁹, Paolo Frezzotti⁹⁰, Daniela Paoli⁹¹, Erika Salvi⁹², Paolo Manunta⁹³, Yosai Mori⁹⁴, Kazunori Miyata⁹⁴, Tomomi Higashide³⁸, Etsuo Chihara⁹⁵, Satoshi Ishiko⁹⁶, Akitoshi

Yoshida⁹⁷, Masahide Yanagi⁹⁸, Yoshiaki Kiuchi⁹⁸, Tsutomu Ohashi⁹⁹, Toshiya Sakurai¹⁰⁰, Takako Sugimoto⁵, Hideki Chuman⁵, Makoto Aihara¹⁰¹, Masaru Inatani¹⁰², Masahiro Miyake^{47,103}, Norimoto Gotoh¹⁰⁴, Fumihiko Matsuda¹⁰⁴, Nagahisa Yoshimura^{47,105}, Yoko Ikeda¹⁹, Morio Ueno¹⁹, Chie Sotozono¹⁹, Jin Wook Jeoung⁴⁵, Min Sagong⁴⁶, Kyu Hyung Park¹⁰⁶, Jeeyun Ahn¹⁰⁷, Marisa Cruz-Aguilar⁴⁹, Sidi M Ezzouhairi⁴², Abderrahman Rafei¹⁰⁸, Yaan Fun Chong¹, Xiao Yu Ng¹, Shuang Ru Goh¹, Yueming Chen¹, Victor H.K. Yong¹, Muhammad Imran Khan¹⁰⁹, Olusola O Olawoye^{110,111}, Adeyinka O Ashaye^{110,111}, Idakwo Ugbede¹¹², Adeola Onakoya^{113,114}, Nkiru Kizor-Akaraiwe^{115,116}, Chaiwat Teekhasaene¹¹⁷, Yanin Suwan¹¹⁷, Wasu Supakontanasan¹¹⁷, Suhanya Okeke^{115,116}, Nkechi Uche^{116,118}, Ifeoma Asimadu¹¹⁵, Humaira Ayub¹¹⁹, Farah Akhtar¹²⁰, Ewa Kosior-Jarecka³², Urszula Lukasik³², Ignacio Lischinsky¹²¹, Vania Castro¹²², Rodolfo Perez Grossmann¹²³, Gordana Sunaric Megevan¹²⁴, Sylvain Roy¹²⁴, Edward Dervan¹²⁵, Eoin Silke¹²⁵, Aparna Rao¹²⁶, Priti Sahay¹²⁶, Pablo Fornero¹²⁷, Osvaldo Cuello¹²⁷, Delia Sivori⁴¹, Tamara Zompa¹²⁸, Richard A Mills¹⁶, Emmanuelle Souzeau¹⁶, Paul Mitchell¹²⁹, Jie Jin Wang¹²⁹, Alex W Hewitt^{17,130}, Michael Coote¹³⁰, Jonathan G Crowston¹³⁰, Sergei Y. Astakhov¹³, Eugeny L. Akopov¹³, Anton Emelyanov^{13,131}, Vera Vysochinskaya¹³¹, Gyulli Kazakbaeva⁴⁴, Rinat Fayzrakhmanov⁴⁴, Saleh A. Al-Obeidan²⁰, Ohoud Owaidhah⁵⁷, Leyla Ali Aljasim⁵⁷, Balram Chowbay^{132,133,134}, Jia Nee Foo^{24,135}, Raphael Q Soh²⁴, Kar Seng Sim²⁴, Zhicheng Xie²⁴, Augustine W.O. Cheong²⁴, Shi Qi Mok²⁴, Hui Meng Soo²⁴, Xiao Yin Chen²⁴, Su Qin Peh²⁴, Khai Koon Heng²⁴, Rahat Husain², Su-Ling Ho¹³⁶, Axel M. Hillmer²⁴, Ching-Yu Cheng^{1,2,3,6}, Francisco A. Escudero-Domínguez⁵⁹, Rogelio González-Sarmiento^{60,137}, Frederico Martinon-Torres^{138,139}, Antonio Salas^{140,141}, Kessara Pathanapitoon¹⁴², Linda Hansapinyo¹⁴², Boonsong Wanichwecharugruang¹⁴³, Naris Kitnarong¹⁴⁴, Anavaj Sakuntabhai^{145,146}, Hiệp X Nguyễn⁵⁶, Giang T.T. Nguyễn⁵⁶, Trình V Nguyễn⁵⁶, Werner Zenz¹⁴⁷, Alexander Binder¹⁴⁷, Daniela S. Klobassa¹⁴⁷, Martin L. Hibberd^{24,148}, Sonia Davila²⁴, Stefan Herms^{149,150,151}, Markus M Nöthen^{149,152}, Susanne Moebus¹⁵³, Robyn M Rautenbach¹⁵⁴, Ari Ziskind¹⁵⁴, Trevor R Carmichael¹², Michele Ramsay¹⁵⁵, Lydia Álvarez^{35,36}, Montserrat García^{35,36}, Héctor González-Iglesias^{35,36}, Pedro P. Rodríguez-Calvo^{35,36}, Luis Fernández-Vega Cueto^{35,36}, Çilingir Oguz¹⁵⁶, Nevbahar Tamcelik¹⁵⁷, Eray Atalay^{1,157}, Bilge Batu¹⁵⁷, Dilek Aktas¹⁵⁸, Burcu Kasim³⁴, M. Roy Wilson¹⁵⁹, Anne L Coleman¹⁶⁰, Yutao Liu¹⁶¹, Pratap Challa²², Leon Herndon²², Rachel W. Kuchtey¹⁶², John Kuchtey¹⁶², Karen Curtin⁶⁵, Craig J. Chaya⁶⁵, Alan Crandall⁶⁵, Linda M. Zangwill¹⁶³, Tien Yin Wong^{1,2,3}, Masakazu Nakano¹⁶⁴, Shigeru Kinoshita^{19,165}, Anneke I. den Hollander^{109,166}, Eija Vesti¹⁶⁷, John H Fingert^{168,169}, Richard K. Lee¹⁷⁰, Arthur J. Sit¹⁷¹, Bradford J. Shingleton¹⁷², Ningli Wang^{52,71}, Daniele Cusi¹⁷³, Raheel Qamar^{174,175}, Peter Kraft¹⁷⁶, Margaret A. Pericak-Vance¹⁷⁷, Soumya Raychaudhuri^{178,179,180,181,182}, Steffen Heegaard^{183,184}, Tero Kivelä¹⁸⁵, André Reis⁷⁶, Friedrich E. Kruse⁷, Robert N Weinreb¹⁶³, Louis R. Pasquale^{28,186}, Jonathan L. Haines^{10,187}, Unnur Thorsteinsdottir^{8,188}, Fridbert Jonasson^{188,189,*}, R Rand Allingham^{1,22,*}, Dan Milea^{1,2,6,*}, Robert Ritch^{190,*}, Toshiaki Kubota^{18,*}, Kei Tashiro^{164,*}, Eranga N Vithana^{1,3,*}, Shazia Micheal^{166,*}, Fotis Topouzis^{79,*}, Jamie E. Craig^{16,*}, Michael

Dubina^{13,131,*}, Periasamy Sundaresan^{191,*}, Kari Stefansson^{8,188,*}, Janey L Wiggs^{186,*}, Francesca Pasutto^{76,*}, Chiea Chuen Khor^{1,24,192,*}

Affiliations

¹Singapore Eye Research Institute, Singapore ²Singapore National Eye Center, Singapore ³Dept of Ophthalmology, Yong Loo Lin School of Medicine, National University of Singapore, Singapore ⁴Ozaki Eye Hospital, Hyuga, Miyazaki, Japan. ⁵Department of Ophthalmology, Faculty of Medicine University of Miyazaki, Miyazaki, Japan ⁶Academic Clinical Program for Ophthalmology and Visual Sciences, Office of Clinical & Academic Faculty Affairs, Duke-NUS Graduate Medical School, Singapore ⁷Department of Ophthalmology, Universitätsklinikum Erlangen, Friedrich-Alexander-Universität Erlangen-Nürnberg, Erlangen, Germany ⁸deCODE genetics, Sturlugata 8, 101 Reykjavic, Iceland ⁹Mizoguchi Eye Hospital, Sasebo, Japan. ¹⁰Department of Population and Quantitative Health Sciences, Case Western Reserve University, Cleveland, Ohio, USA. ¹¹Aravind Eye Hospital, Madurai, India. ¹²Division of Ophthalmology, University of the Witwatersrand, Johannesburg, South Africa. ¹³Pavlov First Saint Petersburg State Medical University, St. Petersburg, Russia ¹⁴Department of Ophthalmology, Dalhousie University, Halifax, Nova Scotia, Canada ¹⁵Department of Pathology, Dalhousie University, Halifax, Nova Scotia, Canada ¹⁶Department of Ophthalmology, Flinders University, Adelaide, SA, Australia ¹⁷Menzies Institute for Medical Research, University of Tasmania, Australia ¹⁸Department of Ophthalmology, Oita University Faculty of Medicine, Oita, Japan ¹⁹Department of Ophthalmology, Kyoto Prefectural University of Medicine, Kyoto, Japan. ²⁰Department of Ophthalmology, College of Medicine, King Saud University, Riyadh, Saudi Arabia ²¹Department of Ophthalmology, College of Medicine, University of Florida, Jacksonville, FL, USA ²²Department of Ophthalmology, Duke University Eye Center, Durham, NC, USA ²³Department of Medicine, Duke University Medical Center, Durham, NC, USA ²⁴Genome Institute of Singapore, Singapore ²⁵Department of Genetics, Aravind Medical Research Foundation, Madurai, India ²⁶“Carol Davila” University of Medicine and Pharmacy, Bucharest, Romania ²⁷University Emergency Hospital, Department of Ophthalmology, Bucharest, Romania ²⁸Channing Division of Network Medicine, Brigham and Women’s Hospital, Harvard Medical School, Boston, Massachusetts, USA ²⁹Department of Biostatistics, University of Washington, Seattle, WA, USA ³⁰Hayashi Eye Hospital, 23-35, Hakataekimae-4, Hakata-ku, Fukuoka, Japan ³¹Shinjo Eye Clinic, 889-1, Mego, Simokitakatamachi, Miyazaki-shi, Miyazaki, Japan ³²Department of Diagnostics and Microsurgery of Glaucoma, Medical University, Lublin, Poland, Chmielna 1, 20-079 Lublin, Poland. ³³Inoue Eye Hospital, 4-3 Kanda-Surugadai, Chiyoda-ku, Tokyo, Japan. ³⁴Department of Ophthalmology, Hacettepe University, Faculty of Medicine, Ankara, Turkey ³⁵Fernández-Vega University Institute and Foundation of Ophthalmological Research, University of Oviedo, Oviedo, Spain. ³⁶Fernández-Vega Ophthalmological Institute, Avda. Dres. Fernández-Vega, 34, Oviedo 33012, Spain ³⁷Department of Ophthalmology and Visual Science, Yale University School of Medicine, 300 George St, 8100A, New Haven, CT 06510, USA. ³⁸Department of

Ophthalmology Kanazawa University Graduate School of Medical Science, 13-1 Takara-machi, Kanazawa, Japan ³⁹. Department of Medical Genetics, University of Helsinki, Helsinki, Finland. ⁴⁰. Organización Médica de Investigación, Uruguay 725 - PB, Buenos Aires, Argentina ⁴¹. Fundacion para el Estudio del Glaucoma, Marcelo T de Alvear 2010 - 2A, Buenos Aires, Argentina ⁴². Clinique Spécialisée en Ophtalmologie Mohammedia, Mohammedia, Morocco ⁴³. Department of Ophthalmology, Eskisehir Osmangazi University, Meselik, Eskisehir, Turkey ⁴⁴. Ufa Eye Research Institute, Ufa, Republic of Bashkortostan, Russia. ⁴⁵. Department of Ophthalmology, Seoul National University Hospital, Seoul National University College of Medicine, Seoul, South Korea ⁴⁶. Department of Ophthalmology, Yeungnam University College of Medicine, Daegu, South Korea ⁴⁷. Department of Ophthalmology and Visual Sciences, Kyoto University Graduate School of Medicine, Kyoto, Japan ⁴⁸. Department of Ophthalmology, Otsu Red Cross Hospital, Otsu, Japan 520-8511 ⁴⁹. Genetics Department, Institute of Ophthalmology "Conde de Valenciana" Mexico City, Mexico, Chimalpopoca 14, Col. Obrera, CP 06800, Mexico City, Mexico ⁵⁰. Biochemistry Department, Faculty of Medicine, UNAM, Mexico City, Mexico ⁵¹. Department of Ophthalmology, Medical Faculty Mannheim of the Ruprecht-Karls-University of Heidelberg, Mannheim, Germany. ⁵². Beijing Institute of Ophthalmology and Visual Science Key Lab Beijing-China, Beijing Tongren Eye Center, Beijing Tongren Hospital, Capital Medical University, Beijing, China ⁵³. Narayana Nethralaya Eye Hospital, 121/C, Chord Road, Rajajinagar, 1st R Block, Bangalore 560 010, India. ⁵⁴. Chichua Medical Center Mzera LLC, Tbilisi, Georgia ⁵⁵. Jadhavbhai Nathamal Singhvi Department of Glaucoma, Medical Research Foundation, Sankara Nethralaya, 18, College Road, Chennai, India ⁵⁶. Vietnam National Institute of Ophthalmology, Hanoi, Vietnam ⁵⁷. King Khaled Eye Specialist Hospital, Riyadh, Kingdom of Saudi Arabia ⁵⁸. Department of Ophthalmology and Visual Sciences, Illinois Eye and Ear Infirmary, College of Medicine, University of Illinois at Chicago, Chicago, IL, United States ⁵⁹. Department of Ophthalmology, University Hospital of Salamanca, Salamanca, Spain ⁶⁰. Institute for Biomedical Research of Salamanca (IBSAL), Spain ⁶¹. Ophthalmic Research Center, Shahid Beheshti University of Medical Sciences, Tehran, Iran ⁶². Farabi eye hospital, Tehran University Eye Research Center. Tehran University of Medical Sciences, Tehran, Iran. ⁶³. Ideta Eye Hospital, Kumamoto City, Japan. ⁶⁴. Eye Clinic, Rigshospitalet - Glostrup, Denmark ⁶⁵. John A. Moran Eye Center, Dept. of Ophthalmology, University of Utah, Salt Lake City, Utah, USA ⁶⁶. Sichuan Provincial Key Laboratory for Human Disease Gene Study, Sichuan Provincial People's Hospital, University of Electronic Science and Technology of China, Chengdu, Sichuan, China. ⁶⁷. School of Medicine, University of Electronic Science and Technology of China, Chengdu, Sichuan, China. ⁶⁸. Department of Ophthalmology, the First Affiliated Hospital of Xinjiang Medical University, Urumchi 830054; 2 Xinjiang Uygur Autonomous Region, China ⁶⁹. Center for Human Molecular Biology & Genetics, The Institute of Laboratory Medicine, Sichuan Academy of Medical Sciences & Sichuan Provincial People's Hospital, Chengdu, Sichuan, China. ⁷⁰. Sichuan Translational Research Hospital, Chinese Academy of Sciences, Chengdu 610072, Sichuan, China

⁷¹·Beijing Tongren Eye Center, Beijing Tongren Hospital, Capital Medical University, Beijing Ophthalmology & Visual Science Key Lab, Beijing, China ⁷²·Shenzhen Key Laboratory of Ophthalmology, Shenzhen Eye Hospital, Jinan University, Shenzhen, China. ⁷³·Département d'Ophtalmologie, Centre Hospitalier Universitaire, F-49933 Angers, France ⁷⁴·Département de Biochimie et Génétique, Centre Hospitalier Universitaire, F-49933 Angers, France ⁷⁵·David Tvildiani Medical University, Tbilisi, Georgia ⁷⁶·Institute of Human Genetics, Friedrich-Alexander-Universität, Erlangen-Nürnberg, Erlangen, Germany ⁷⁷·Department of Ophthalmology, Medical University Graz, Graz, Austria ⁷⁸·Institute for Ophthalmic Research, Centre for Ophthalmology, University of Tuebingen, Tuebingen, Germany. ⁷⁹·Department of Ophthalmology, School of Medicine, Aristotle University of Thessaloniki, Thessaloniki, Greece ⁸⁰·Laboratory of General Biology, School of Medicine, Aristotle University of Thessaloniki, Thessaloniki, Greece ⁸¹·GROW Research Lab, Narayana Nethralaya Foundation, Bangalore, India ⁸²·Narayana Nethralaya Eye Hospital, 121/C, Chord Road, Rajajinagar, 1st R Block, Bangalore 560 010, India. ⁸³·Santa Lucia Eye Hospital from Buenos Aires, Argentina. ⁸⁴·Aravind Eye Hospital, Pondicherry, India ⁸⁵·Aravind Eye Hospital, Tirunelveli, India ⁸⁶·Aravind Eye Hospital, Coimbatore, India ⁸⁷·Vision Research Foundation, 18, College Road, Chennai, India ⁸⁸·Ocular Tissue Engineering Research Center, Shahid Beheshti University of Medical Sciences, Tehran, Iran ⁸⁹·Dipartimento di Scienze Chirurgiche, Università di Torino, Turin, Italy. ⁹⁰·Ophthalmology Unit Department of Medicine, Surgery and Neuroscience, University of Siena, Siena, Italy ⁹¹·Department of Ophthalmology, Monfalcone Hospital, Gorizia, Italy ⁹²·Department of Health Sciences, University of Milan, Italy ⁹³·Department of Nephrology, University Vita-Salute San Raffaele, Milano, Italy ⁹⁴·Miyata Eye Hospital, 6-3, Kurahara, Miyakonojo, Miyazaki 885-0051 Japan ⁹⁵·Sensho-kai Eye Institute, Minamiyama 50-1, Iseda, Uji, Kyoto 611-0043, Japan ⁹⁶·Department of Medicine and Engineering Combined Research Institute, Asahikawa Medical University, Japan ⁹⁷·Department of Ophthalmology, Asahikawa Medical University, 4-5 Nishikagura, Asahikawa 078-8510 Japan ⁹⁸·Hiroshima University, Department of Ophthalmology and Visual Sciences, 1-2-3 Kasumi, Minami-ku, Hiroshima, 734-8551, Japan ⁹⁹·Ohashi eye center, Kita2-1 Hondori6 Shiroishi-ku Sapporo 003-0027 Japan ¹⁰⁰·Tane Memorial Eye Hospital, 1-1-39, Sakaigawa, Nishi-ku, Osaka, 550-0024, Japan ¹⁰¹·Department of Ophthalmology, University of Tokyo, Bunkyo, Tokyo 113-8655, Japan ¹⁰²·Department of Ophthalmology, Faculty of Medical Science, University of Fukui, 23-3 Shimoaizuki, Matsuoka, Eiheiji, Yoshida, Fukui, 910-1193, Japan ¹⁰³·Japan Agency for Medical Research and Development, Tokyo, Japan 100-0004 ¹⁰⁴·Center for Genomic Medicine/Inserm U.852, Kyoto University Graduate School of Medicine, Kyoto, Japan 606-8507 ¹⁰⁵·Tazuke Kofukai Foundation, Medical Research Institute, Kitano Hospital, Osaka, Japan 530-8480 ¹⁰⁶·Department of Ophthalmology, Seoul National University Bundang Hospital, Gyeonggi, South Korea. ¹⁰⁷·Department of Ophthalmology, Seoul Metropolitan Government Seoul National University Boramae Medical Center, Seoul, South Korea. ¹⁰⁸·Laboratoires RAFAI, Mohammedia, Morocco ¹⁰⁹·Department of Human Genetics, Radboud University Medical Centre,

Nijmegen, the Netherlands ¹¹⁰.Department of Ophthalmology, College of Medicine, University of Ibadan, Ibadan, Nigeria ¹¹¹.Department of Ophthalmology, University College Hospital, Ibadan, Nigeria ¹¹².ECWA Eye Hospital, Kano, Nigeria ¹¹³.Department of Ophthalmology University of Lagos, Lagos, Nigeria ¹¹⁴.Guinness Eye Centre Lagos University Teaching Hospital, Lagos Nigeria ¹¹⁵.Department of Ophthalmology, ESUT Teaching Hospital Parklane, Park Avenue, GRA. Enugu, Nigeria ¹¹⁶.The Eye Specialists Hospital, 11 Church View, GRA, Enugu, Nigeria. ¹¹⁷.Ramathibodi Hospital, Mahidol University, Bangkok, Thailand ¹¹⁸.Department of Ophthalmology, University of Nigeria Teaching Hospital, Ituku-Ozalla, Enugu, Nigeria. ¹¹⁹.Department of Environmental Sciences, COMSATS Institute of Information Technology, Abbottabad Campus, Pakistan. ¹²⁰.Pakistan Institute of Ophthalmology, Al-Shifa Trust Eye Hospital, Rawalpindi, Pakistan ¹²¹.Centro Oftalmologico Lischinsky, Tucuman, Argentina ¹²².Universidad Peruana Cayetano Heredia- Hospital Nacional Arzobispo Loayza, Lima - Perú. ¹²³.Instituto de Glaucoma y Catarata, Lima - Perú ¹²⁴.Clinical Research Centre Adolphe de Rothschild , Société Médicale de Beaulieu, Geneva, Switzerland. ¹²⁵.Mater Misericordiae University Hospital, Eccles St, Dublin 7, Ireland ¹²⁶.Shri Mithu Tulsi Chanrai campus, LV Prasad Eye Institute, Patia, Bhubaneswar, Odisha, India ¹²⁷.Hospital Cordoba, Cordoba, Argentina ¹²⁸.Centro Oftalmologico Charles, Buenos Aires, Argentina ¹²⁹.Centre for Vision Research, Department of Ophthalmology and Westmead Institute for Medical Research, University of Sydney, NSW Australia ¹³⁰.Centre for Eye Research Australia (CERA), University of Melbourne, Royal Victorian Eye and Ear Hospital, Melbourne, Victoria, Australia ¹³¹.St. Petersburg Academic University, St. Petersburg, Russia ¹³².Clinical Pharmacology, SingHealth, Singapore, Singapore ¹³³.Clinical Pharmacology Laboratory, National Cancer Centre, Singapore ¹³⁴.Office of Clinical Sciences, Duke-NUS Medical School, Singapore ¹³⁵.Lee Kong Chian School of Medicine, Nanyang Technological University, Singapore. ¹³⁶.Department of Ophthalmology, Tan Tock Seng Hospital, Singapore ¹³⁷.Molecular Medicine Unit. Department of Medicine. University of Salamanca. Salamanca, Spain ¹³⁸.Translational Pediatrics and Infectious Diseases, Hospital Clínico Universitario de Santiago, Santiago de Compostela, Spain ¹³⁹.GENVIP Research Group, Instituto de Investigación Sanitaria de Santiago, Galicia, Spain ¹⁴⁰.Unidade de Xenética, Departamento de Anatomía Patolóxica e Ciencias Forenses, Spain ¹⁴¹.Instituto de Ciencias Forenses, Facultade de Medicina, Universidade de Santiago de Compostela, Santiago de Compostela, Galicia, Spain. ¹⁴².Department of Ophthalmology, Faculty of Medicine, Chiang Mai University, Chiang Mai, Thailand ¹⁴³.Department of Ophthalmology, Rajavithi Hospital, Bangkok, Thailand ¹⁴⁴.Department of Ophthalmology, Faculty of Medicine Siriraj Hospital, Mahidol University, Bangkok, Thailand. ¹⁴⁵.Institute Pasteur, Functional Genetics of Infectious Diseases Unit, Department of Genomes and Genetics, Paris, 75015, France ¹⁴⁶.Centre National de la Recherche Scientifique, Unité de Recherche Associée 3012, Paris, France. ¹⁴⁷.Department of General Pediatrics, Medical University of Graz, Graz, Austria ¹⁴⁸.Faculty of Infectious and Tropical Disease, London School of Hygiene and Tropical Medicine, Keppel Street,

London, WC1E 7HT, UK ¹⁴⁹.Department of Genomics, Life & Brain Center, University of Bonn, Bonn, Germany ¹⁵⁰.Department of Biomedicine, University of Basel, Basel, Switzerland ¹⁵¹.Division of Medical Genetics, University Hospital Basel, Basel, Switzerland ¹⁵².Institute of Human Genetics, University of Bonn, Bonn, Germany ¹⁵³.Institute for Medical Informatics, Biometry and Epidemiology, University Hospital of Essen, University Duisburg-Essen, Essen, Germany ¹⁵⁴.Division of Ophthalmology, Stellenbosch University and Tygerberg Hospital, Cape Town, South Africa ¹⁵⁵.Sydney Brenner Institute for Molecular Bioscience, Faculty of Health Sciences, University of the Witwatersrand, Johannesburg, South Africa ¹⁵⁶.Department of Genetics, Eskisehir Osmangazi University, Meselik, Eskisehir, Turkey. ¹⁵⁷.Istanbul University Cerrahpasa Faculty of Medicine, Istanbul, Turkey. ¹⁵⁸.DAMAGEN Genetic Diagnostic Center, Ankara, Turkey ¹⁵⁹.School of Medicine, Wayne State University, Detroit, Michigan, USA ¹⁶⁰.Center for Community Outreach and Policy, Stein Eye Institute, David Geffen School of Medicine at UCLA, Los Angeles, CA 90095 USA ¹⁶¹.Department of Cellular Biology and Anatomy, Center for Biotechnology and Genomic Medicine, James & Jean Culver Discovery Institute, Augusta University, Augusta, Georgia, USA. ¹⁶².Vanderbilt Eye Institute, Vanderbilt University Medical Center, Nashville, Tennessee 37232-8808, USA ¹⁶³.Hamilton Glaucoma Center, Department of Ophthalmology and Shiley Eye Institute, University of California, San Diego, USA ¹⁶⁴.Department of Genomic Medical Sciences, Kyoto Prefectural University of Medicine, Kyoto, Japan ¹⁶⁵.Department of Frontier Medical Science and Technology for Ophthalmology, Kyoto Prefectural University of Medicine, Kyoto, Japan ¹⁶⁶.Department of Ophthalmology, Radboud University Medical Centre; Nijmegen, the Netherlands ¹⁶⁷.Department of Ophthalmology, University of Turku and Turku University Hospital, Turku, Finland ¹⁶⁸.Institute for Vision Research, University of Iowa, Iowa City, USA ¹⁶⁹.Department of Ophthalmology and Visual Sciences, Carver College of Medicine, University of Iowa, Iowa City, USA ¹⁷⁰.Bascom Palmer Eye Institute, University of Miami Miller School of Medicine, Miami, Florida, USA. ¹⁷¹.Department of Ophthalmology, Mayo Clinic, Rochester, Minnesota, USA ¹⁷².Ophthalmic consultants of Boston, Boston, MA, USA ¹⁷³.Institute of Biomedical Technologies, Italian National Research Centre (ITB-CNR), Segrate-Milano, Italy. ¹⁷⁴.Department of Biosciences, COMSATS Institute of Information Technology, Islamabad Campus, Park Road, Tarlai Kalan, Islamabad, Pakistan ¹⁷⁵.Department of Biochemistry, Al-Nafees Medical College & Hospital, Isra University, Islamabad, Pakistan ¹⁷⁶.Department of Epidemiology, Harvard T.H. Chan School of Public Health, Boston, Massachusetts, USA ¹⁷⁷.John P. Hussman Institute for Human Genomics, University of Miami Miller School of Medicine, Miami, Florida, USA ¹⁷⁸.Divisions of Genetics and Rheumatology, Department of Medicine, Brigham and Women's Hospital and Harvard Medical School, Boston, USA ¹⁷⁹.Partners Center for Personalized Genetic Medicine, Boston, USA ¹⁸⁰.Program in Medical and Population Genetics, Broad Institute of MIT and Harvard, Cambridge, USA ¹⁸¹.Institute of Inflammation and Repair, University of Manchester, Manchester, UK ¹⁸².Rheumatology Unit, Department of Medicine, Karolinska Institutet and Karolinska University Hospital Solna, Stockholm, Sweden.

¹⁸³.Department of Ophthalmology, Rigshospitalet, University of Copenhagen, Denmark. ¹⁸⁴.Department of Pathology, Rigshospitalet, Eye Pathology Section, University of Copenhagen, Denmark. ¹⁸⁵.Department of Ophthalmology, University of Helsinki and Helsinki University Hospital, Helsinki, Finland ¹⁸⁶.Department of Ophthalmology, Harvard Medical School, Massachusetts Eye and Ear Infirmary, Boston, Massachusetts, USA. ¹⁸⁷.Institute of Computational Biology, Case Western Reserve University, Cleveland, Ohio, USA. ¹⁸⁸.Faculty of Medicine, University of Iceland, Reykjavik, Iceland; ¹⁸⁹.Department of Ophthalmology, Landspítali University Hospital, Reykjavik, Iceland ¹⁹⁰.Einhorn Clinical Research Center, New York Eye and Ear Infirmary of Mount Sinai, New York, NY USA ¹⁹¹.Dr. G.Venkataswamy Eye Research Institute, Aravind Medical Research Foundation, Aravind Eye Hospital, No.1 Anna Nagar, Madurai-625 020, Tamilnadu, India ¹⁹².Department of Biochemistry, Yong Loo Lin School of Medicine, National University of Singapore, Singapore

Acknowledgments

This research is supported by the Biomedical Research Council, Agency for Science, Technology, and Research, Singapore (to C.C.K.), by the Glaucoma Foundation of New York (to C.C.K.), by grants from the National Medical Research Council, Singapore (NMRC/TCR/002-SERI/2008 to T.A. and NMRC/CBRG/0032/2013 to E.N.V.), by the Interdisziplinäres Zentrum für Klinische Forschung (IZKF-E23) from Germany to F.P. and to U.S.-S, and by grants from the National Institutes of Health, USA: UM1 CA186107, R01 CA49449, R01 EY015473 to J.L.W. For XFS cases in the USA GWAS dataset, genotyping services were provided through a grant to J.L.W. (HG008597) by the Center for Inherited Disease Research (CIDR). CIDR is fully funded through a federal contract from the National Institutes of Health to The Johns Hopkins University, contract number HHSN268201200008I. We dedicate this article to the ophthalmologist Eva Forsman from Finland, who passed away after diagnosing all of the exfoliation syndrome cases from Finland.

References

1. Vesti E & Kivela T Exfoliation syndrome and exfoliation glaucoma. *Prog Retin Eye Res* 19, 345–68 (2000). [PubMed: 10749381]
2. Ritch R & Schlotzer-Schrehardt U Exfoliation syndrome. *Surv Ophthalmol* 45, 265–315 (2001). [PubMed: 11166342]
3. Leske MC et al. Factors for glaucoma progression and the effect of treatment: the early manifest glaucoma trial. *Arch Ophthalmol* 121, 48–56 (2003). [PubMed: 12523884]
4. Ritch R, Schlotzer-Schrehardt U & Konstas AG Why is glaucoma associated with exfoliation syndrome? *Prog Retin Eye Res* 22, 253–75 (2003). [PubMed: 12852486]
5. Olawoye OO et al. Exfoliation syndrome in Nigeria. *Middle East Afr J Ophthalmol* 19, 402–5 (2012). [PubMed: 23248543]
6. Kivela T Ocular Pseudoexfoliation Syndrome and Life Span: Act 2. *EBioMedicine* 2, 640–1 (2015). [PubMed: 26288835]
7. Ritch R Ocular and systemic manifestations of exfoliation syndrome. *J Glaucoma* 23, S1–8 (2014).
8. Ritch R Exfoliation syndrome-the most common identifiable cause of open-angle glaucoma. *J Glaucoma* 3, 176–7 (1994). [PubMed: 19920577]
9. Allingham RR et al. Pseudoexfoliation syndrome in Icelandic families. *Br J Ophthalmol* 85, 702–7 (2001). [PubMed: 11371492]
10. Orr AC et al. Exfoliation syndrome: clinical and genetic features. *Ophthalmic Genet* 22, 171–85 (2001). [PubMed: 11559859]
11. Thorleifsson G et al. Common sequence variants in the LOXL1 gene confer susceptibility to exfoliation glaucoma. *Science* 317, 1397–400 (2007). [PubMed: 17690259]

12. Williams SE et al. Major LOXL1 risk allele is reversed in exfoliation glaucoma in a black South African population. *Mol Vis* 16, 705–12 (2010). [PubMed: 20431720]
13. Wiggs JL & Pasquale LR Expression and regulation of LOXL1 and elastin-related genes in eyes with exfoliation syndrome. *J Glaucoma* 23, S62–3 (2014). [PubMed: 25275910]
14. Aung Tet et al. A common variant mapping to CACNA1A is associated with susceptibility to exfoliation syndrome. *Nat Genet* 47, 387–92 (2015). [PubMed: 25706626]
15. Al Olama AA et al. A meta-analysis of 87,040 individuals identifies 23 new susceptibility loci for prostate cancer. *Nat Genet* 46, 1103–9 (2014). [PubMed: 25217961]
16. Liu JZ et al. Association analyses identify 38 susceptibility loci for inflammatory bowel disease and highlight shared genetic risk across populations. *Nat Genet* 47, 979–86 (2015). [PubMed: 26192919]
17. Paternoster Let et al. Multi-ancestry genome-wide association study of 21,000 cases and 95,000 controls identifies new risk loci for atopic dermatitis. *Nat Genet* 47, 1449–56 (2015). [PubMed: 26482879]
18. Ehret GB et al. The genetics of blood pressure regulation and its target organs from association studies in 342,415 individuals. *Nat Genet* (2016).
19. Liu Cet et al. Meta-analysis identifies common and rare variants influencing blood pressure and overlapping with metabolic trait loci. *Nat Genet* (2016).
20. Surendran Pet et al. Trans-ancestry meta-analyses identify rare and common variants associated with blood pressure and hypertension. *Nat Genet* (2016).
21. Hauser MA et al. Genetic variants and cellular stressors associated with exfoliation syndrome modulate promoter activity of a lncRNA within the LOXL1 locus. *Hum Mol Genet* 24, 6552–63 (2015). [PubMed: 26307087]
22. Chen Het et al. Ethnicity-based subgroup meta-analysis of the association of LOXL1 polymorphisms with glaucoma. *Mol Vis* 16, 167–77 (2010). [PubMed: 20142848]
23. Fan BJ et al. LOXL1 promoter haplotypes are associated with exfoliation syndrome in a U.S. Caucasian population. *Invest Ophthalmol Vis Sci* 52, 2372–8 (2011). [PubMed: 21212179]
24. Ozaki Met et al. Association of LOXL1 gene polymorphisms with pseudoexfoliation in the Japanese. *Invest Ophthalmol Vis Sci* 49, 3976–80 (2008). [PubMed: 18450598]
25. Tanito Met et al. LOXL1 variants in elderly Japanese patients with exfoliation syndrome/glaucoma, primary open-angle glaucoma, normal tension glaucoma, and cataract. *Mol Vis* 14, 1898–905 (2008). [PubMed: 18958304]
26. Pasutto Fet et al. Association of LOXL1 common sequence variants in German and Italian patients with pseudoexfoliation syndrome and pseudoexfoliation glaucoma. *Invest Ophthalmol Vis Sci* 49, 1459–63 (2008). [PubMed: 18385063]
27. Mori Ket et al. LOXL1 genetic polymorphisms are associated with exfoliation glaucoma in the Japanese population. *Mol Vis* 14, 1037–40 (2008). [PubMed: 18552979]
28. Nakano Met et al. Novel common variants and susceptible haplotype for exfoliation glaucoma specific to Asian population. *Sci Rep* 4, 5340 (2014). [PubMed: 24938310]
29. Flannick Jet et al. Loss-of-function mutations in SLC30A8 protect against type 2 diabetes. *Nat Genet* 46, 357–63 (2014). [PubMed: 24584071]
30. Bonnefond Aet et al. Rare MTNR1B variants impairing melatonin receptor 1B function contribute to type 2 diabetes. *Nat Genet* 44, 297–301 (2012). [PubMed: 22286214]
31. Majithia ARet et al. Rare variants in PPARG with decreased activity in adipocyte differentiation are associated with increased risk of type 2 diabetes. *Proc Natl Acad Sci U S A* 111, 13127–32 (2014). [PubMed: 25157153]
32. Majithia ARet et al. Prospective functional classification of all possible missense variants in PPARG. *Nat Genet* (2016).
33. Do Ret et al. Exome sequencing identifies rare LDLR and APOA5 alleles conferring risk for myocardial infarction. *Nature* 518, 102–6 (2015). [PubMed: 25487149]
34. Luo Yet et al. Exploring the genetic architecture of inflammatory bowel disease by whole-genome sequencing identifies association at ADCY7. *Nat Genet* (2017).

35. Raychaudhuri Set al. A rare penetrant mutation in CFH confers high risk of age-related macular degeneration. *Nat Genet* 43, 1232–6 (2011). [PubMed: 22019782]
36. Seddon JMet al. Rare variants in CFI, C3 and C9 are associated with high risk of advanced age-related macular degeneration. *Nat Genet* 45, 1366–70 (2013). [PubMed: 24036952]
37. Fritsche LGet al. A large genome-wide association study of age-related macular degeneration highlights contributions of rare and common variants. *Nat Genet* 48, 134–43 (2016). [PubMed: 26691988]
38. Schlotzer-Schrehardt U, von der Mark K, Sakai LY & Naumann GO Increased extracellular deposition of fibrillin-containing fibrils in pseudoexfoliation syndrome. *Invest Ophthalmol Vis Sci* 38, 970–84 (1997). [PubMed: 9112993]
39. Schlotzer-Schrehardt U, Zenkel M, Kuchle M, Sakai LY & Naumann GO Role of transforming growth factor-beta1 and its latent form binding protein in pseudoexfoliation syndrome. *Exp Eye Res* 73, 765–80 (2001). [PubMed: 11846508]
40. Schlotzer-Schrehardt U Molecular pathology of pseudoexfoliation syndrome/glaucoma--new insights from LOXL1 gene associations. *Exp Eye Res* 88, 776–85 (2009). [PubMed: 18809397]
41. Lucero HA & Kagan HM Lysyl oxidase: an oxidative enzyme and effector of cell function. *Cell Mol Life Sci* 63, 2304–16 (2006). [PubMed: 16909208]
42. Liu Xet al. Elastic fiber homeostasis requires lysyl oxidase-like 1 protein. *Nat Genet* 36, 178–82 (2004). [PubMed: 14745449]
43. Atienza JMet al. Dynamic and label-free cell-based assays using the real-time cell electronic sensing system. *Assay Drug Dev Technol* 4, 597–607 (2006). [PubMed: 17115930]
44. Solly K, Wang X, Xu X, Strulovici B & Zheng W Application of real-time cell electronic sensing (RT-CES) technology to cell-based assays. *Assay Drug Dev Technol* 2, 363–72 (2004). [PubMed: 15357917]
45. Urcan Eet al. Real-time xCELLigence impedance analysis of the cytotoxicity of dental composite components on human gingival fibroblasts. *Dent Mater* 26, 51–8 (2010). [PubMed: 19767088]
46. Okbay Aet al. Genome-wide association study identifies 74 loci associated with educational attainment. *Nature* 533, 539–42 (2016). [PubMed: 27225129]
47. Schizophrenia Working Group of the Psychiatric Genomics, C. Biological insights from 108 schizophrenia-associated genetic loci. *Nature* 511, 421–7 (2014). [PubMed: 25056061]
48. Gaulton KJet al. Genetic fine mapping and genomic annotation defines causal mechanisms at type 2 diabetes susceptibility loci. *Nat Genet* 47, 1415–25 (2015). [PubMed: 26551672]
49. Wellcome Trust Case Control, C. et al. Bayesian refinement of association signals for 14 loci in 3 common diseases. *Nat Genet* 44, 1294–301 (2012). [PubMed: 23104008]
50. Liu Yet al. Serial analysis of gene expression (SAGE) in normal human trabecular meshwork. *Mol Vis* 17, 885–93 (2011). [PubMed: 21528004]
51. Wagner AHet al. Exon-level expression profiling of ocular tissues. *Exp Eye Res* 111, 105–11(2013). [PubMed: 23500522]
52. Wistow Get al. NEIBank: genomics and bioinformatics resources for vision research. *Mol Vis* 14, 1327–37 (2008). [PubMed: 18648525]
53. Bowes Rickman Cet al. Defining the human macula transcriptome and candidate retinal disease genes using EyeSAGE. *Invest Ophthalmol Vis Sci* 47, 2305–16 (2006). [PubMed: 16723438]
54. Springelkamp Het al. ARHGEF12 influences the risk of glaucoma by increasing intraocular pressure. *Hum Mol Genet* 24, 2689–99 (2015). [PubMed: 25637523]
55. Ward LD & Kellis M HaploReg: a resource for exploring chromatin states, conservation, and regulatory motif alterations within sets of genetically linked variants. *Nucleic Acids Res* 40, D930–4 (2012). [PubMed: 22064851]
56. Westra HJet al. Systematic identification of trans eQTLs as putative drivers of known disease associations. *Nat Genet* 45, 1238–43 (2013). [PubMed: 24013639]
57. Orchard Set al. The MIntAct project--IntAct as a common curation platform for 11 molecular interaction databases. *Nucleic Acids Res* 42, D358–63 (2014). [PubMed: 24234451]
58. Lee PH, O'Dushlaine C, Thomas B & Purcell SM INRICH: interval-based enrichment analysis for genome-wide association studies. *Bioinformatics* 28, 1797–9 (2012). [PubMed: 22513993]

59. Barker HE, Cox TR & Erler JT The rationale for targeting the LOX family in cancer. *Nat Rev Cancer* 12, 540–52 (2012). [PubMed: 22810810]
60. Braunsman Cet al. Evaluation of lamina cribrosa and peripapillary sclera stiffness in pseudoexfoliation and normal eyes by atomic force microscopy. *Invest Ophthalmol Vis Sci* 53, 2960–7 (2012). [PubMed: 22491409]
61. Schlotzer-Schrehardt UM, Dorfler S & Naumann GO Corneal endothelial involvement in pseudoexfoliation syndrome. *Arch Ophthalmol* 111, 666–74 (1993). [PubMed: 8489451]
62. Sauna ZE & Kimchi-Sarfaty C Understanding the contribution of synonymous mutations to human disease. *Nat Rev Genet* 12, 683–91 (2011). [PubMed: 21878961]
63. Shabalina SA, Spiridonov NA & Kashina A Sounds of silence: synonymous nucleotides as a key to biological regulation and complexity. *Nucleic Acids Res* 41, 2073–94 (2013). [PubMed: 23293005]
64. Hunt RC, Simhadri VL, Iandoli M, Sauna ZE & Kimchi-Sarfaty C Exposing synonymous mutations. *Trends Genet* 30, 308–21 (2014). [PubMed: 24954581]
65. Zenkel M, Kruse FE, Naumann GO & Schlotzer-Schrehardt U Impaired cytoprotective mechanisms in eyes with pseudoexfoliation syndrome/glaucoma. *Invest Ophthalmol Vis Sci* 48, 5558–66 (2007). [PubMed: 18055805]
66. Want Aet al. Autophagy and Mitochondrial Dysfunction in Tenon Fibroblasts from Exfoliation Glaucoma Patients. *PLoS One* 11, e0157404 (2016).
67. Korolchuk VI, Menzies FM & Rubinsztein DC Mechanisms of cross-talk between the ubiquitin-proteasome and autophagy-lysosome systems. *FEBS Lett* 584, 1393–8 (2010). [PubMed: 20040365]
68. Kraft C, Peter M & Hofmann K Selective autophagy: ubiquitin-mediated recognition and beyond. *Nat Cell Biol* 12, 836–41 (2010). [PubMed: 20811356]
69. Schlotzer-Schrehardt U & Naumann GO Ocular and systemic pseudoexfoliation syndrome. *Am J Ophthalmol* 141, 921–937 (2006). [PubMed: 16678509]
70. Kivela T, Hietanen J & Uusitalo M Autopsy analysis of clinically unilateral exfoliation syndrome. *Invest Ophthalmol Vis Sci* 38, 2008–15 (1997). [PubMed: 9331264]
71. Guan Wet al. Genome-wide association study of plasma N6 polyunsaturated fatty acids within the cohorts for heart and aging research in genomic epidemiology consortium. *Circ Cardiovasc Genet* 7, 321–31 (2014). [PubMed: 24823311]
72. Lambert JCet al. Meta-analysis of 74,046 individuals identifies 11 new susceptibility loci for Alzheimer's disease. *Nat Genet* 45, 1452–8 (2013). [PubMed: 24162737]
73. Nalls MAet al. Large-scale meta-analysis of genome-wide association data identifies six new risk loci for Parkinson's disease. *Nat Genet* 46, 989–93 (2014). [PubMed: 25064009]
74. Cohen JC, Boerwinkle E, Mosley TH Jr. & Hobbs HH Sequence variations in PCSK9, low LDL, and protection against coronary heart disease. *N Engl J Med* 354, 1264–72 (2006). [PubMed: 16554528]
75. Jonsson Tet al. A mutation in APP protects against Alzheimer's disease and age-related cognitive decline. *Nature* 488, 96–9 (2012). [PubMed: 22801501]
76. Nioi Pet al. Variant ASGR1 Associated with a Reduced Risk of Coronary Artery Disease. *N Engl J Med* 374, 2131–41 (2016). [PubMed: 27192541]
77. Consortium UIGet al. Genome-wide association study of ulcerative colitis identifies three new susceptibility loci, including the HNF4A region. *Nat Genet* 41, 1330–4 (2009). [PubMed: 19915572]
78. Anderson CAet al. Data quality control in genetic case-control association studies. *Nat Protoc* 5, 1564–73 (2010). [PubMed: 21085122]
79. Mells GFet al. Genome-wide association study identifies 12 new susceptibility loci for primary biliary cirrhosis. *Nat Genet* 43, 329–32 (2011). [PubMed: 21399635]
80. Price ALet al. Principal components analysis corrects for stratification in genome-wide association studies. *Nat Genet* 38, 904–9 (2006). [PubMed: 16862161]

81. Verhoeven VJ et al. Genome-wide meta-analyses of multi-ancestry cohorts identify multiple new susceptibility loci for refractive error and myopia. *Nat Genet* 45, 314–8 (2013). [PubMed: 23396134]
82. Kiryluk K et al. Discovery of new risk loci for IgA nephropathy implicates genes involved in immunity against intestinal pathogens. *Nat Genet* 46, 1187–96 (2014). [PubMed: 25305756]
83. Bronson P et al. Common variants at PVT1, ATG13-AMBRA1, AHI1 and CLEC16A are associated with selective IgA deficiency. *Nat Genet* 48, 1425–1429 (2016). [PubMed: 27723758]
84. Okada Y et al. Genetics of rheumatoid arthritis contributes to biology and drug discovery. *Nature* 506, 376–81 (2014). [PubMed: 24390342]
85. Kooner J et al. Genome-wide association study in individuals of South Asian ancestry identifies six new type 2 diabetes susceptibility loci. *Nat Genet* 43, 984–9 (2011). [PubMed: 21874001]
86. Blake J et al. The Mouse Genome Database: integration of and access to knowledge about the laboratory mouse. *Nucleic Acids Res* 42, D810–7 (2014). [PubMed: 24285300]
87. Foo J et al. Analysis of non-synonymous-coding variants of Parkinson's disease-related pathogenic and susceptibility genes in East Asian populations. *Hum Mol Genet* 23, 3891–7 (2014). [PubMed: 24565865]
88. Cheng T et al. Five endometrial cancer risk loci identified through genome-wide association analysis. *Nat Genet* 48, 667–74 (2016). [PubMed: 27135401]
89. Browning BL & Browning SR A unified approach to genotype imputation and haplotype-phase inference for large data sets of trios and unrelated individuals. *Am J Hum Genet* 84, 210–23 (2009). [PubMed: 19200528]
90. Purcell S et al. PLINK: a tool set for whole-genome association and population-based linkage analyses. *Am J Hum Genet* 81, 559–75 (2007). [PubMed: 17701901]

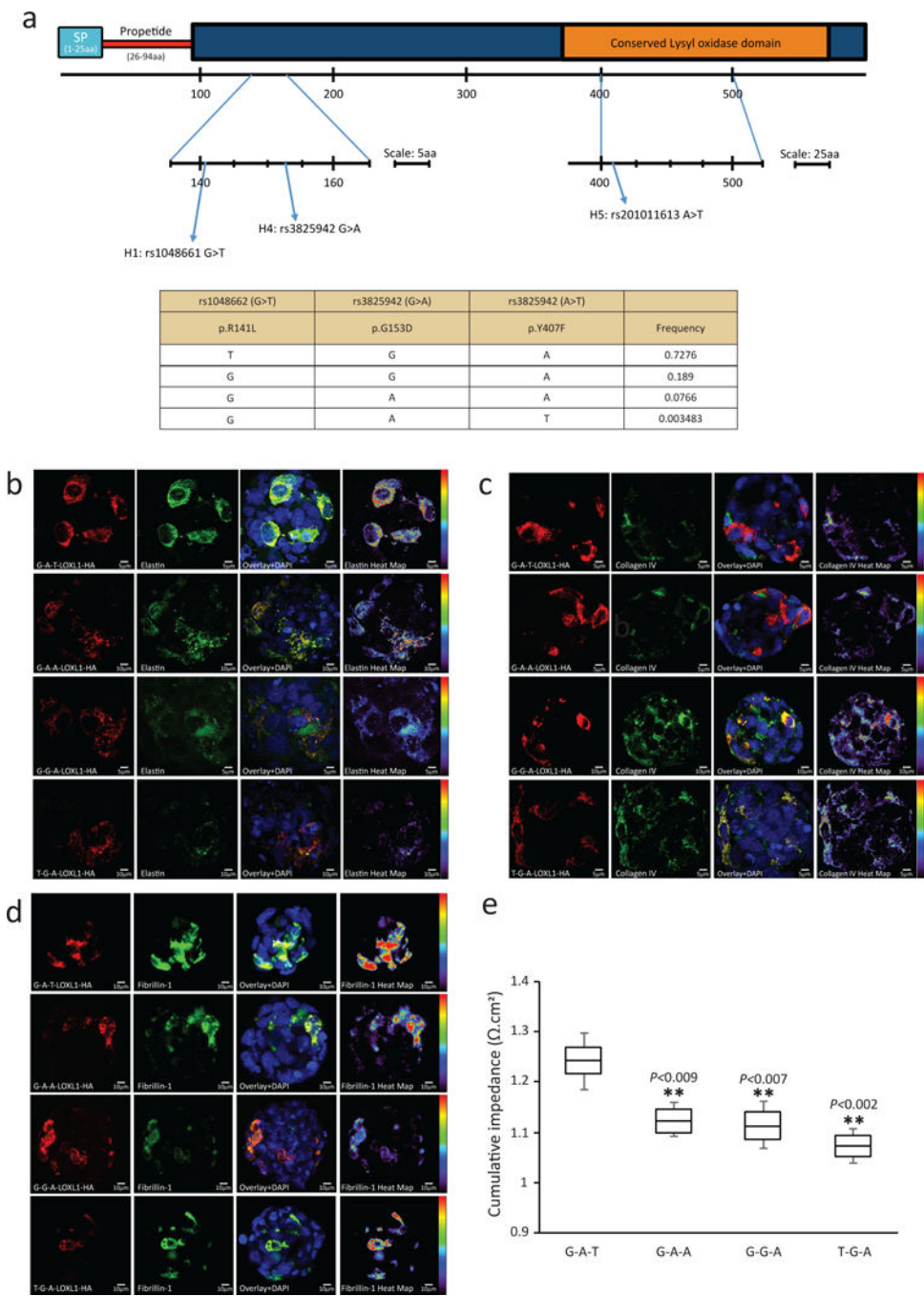


Figure 1.
LOXL1 p.Y407F regulates ECM synthesis and improves cellular adhesion.
(a) Schematic diagram of LOXL1 indicating the protein domain positions for the variants evaluated in this study.
(b) Immunofluorescent staining of HA-tagged LOXL1 variants overexpressed in HLEC cells labelled with anti-HA for detection of overexpressed forms of LOXL1 (red) and elastin (green). Cell nuclei are stained in blue. The heat map for elastin indicates the intensity of elastin staining from red (increased expression) to purple (decreased expression).

- c) Immunofluorescent staining of HA-tagged LOXL1 variants overexpressed in HLEC cells labelled with anti-HA for detection of overexpressed forms of LOXL1 (red) and collagen IV (green). Cell nuclei are stained in blue.. The heat map for collagen IV indicates the intensity of collagen IV staining from red (increased expression) to purple (decreased expression).
- d) Immunofluorescent staining of HA-tagged LOXL1 variants overexpressed in HLEC cells labelled with anti-HA for detection of overexpressed forms of LOXL1 (red) and fibrillin 1 (green). Cell nuclei are stained in blue. The heat map for fibrillin 1 indicates the intensity of fibrillin 1 staining from red (increased expression) to purple (decreased expression).
- e) Cumulative average of impedance values (as a surrogate for cellular adhesion strength) measured over 35h post nucleofection of HLECs overexpressing the four tested *LOXL1* haplotypes. Data represent mean \pm s.e.m. of four independent experiments. ** represents $P < 0.01$ when compared against the rare, protective LOXL1 p.407F-carrying G-A-T haplotype. The four haplotypes tested were LOXL1-(G-A-T), - (G-A-A), -(T-G-A) and -(G-G-A). This experiment was further validated in Supplementary Figure 7.

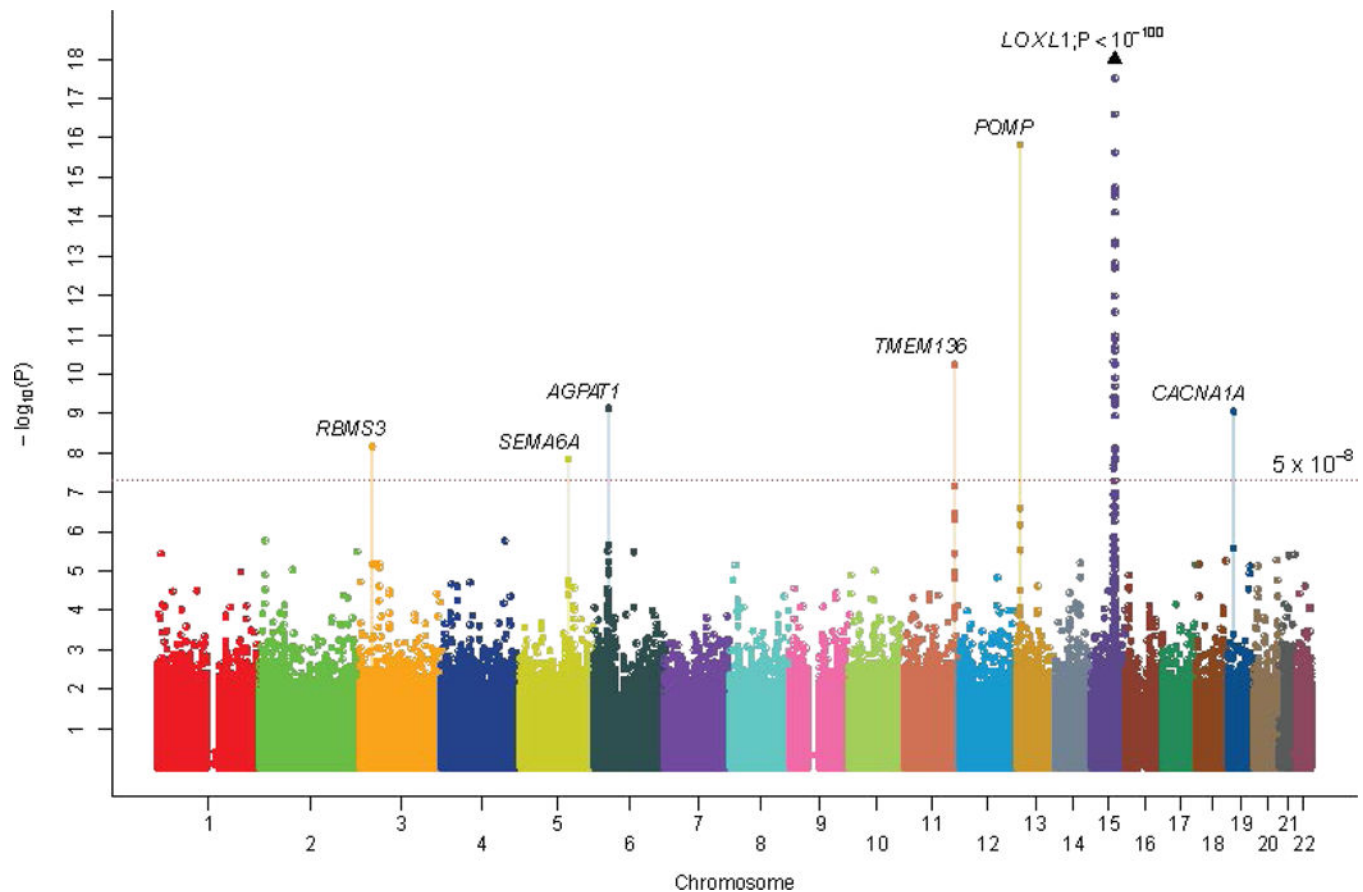
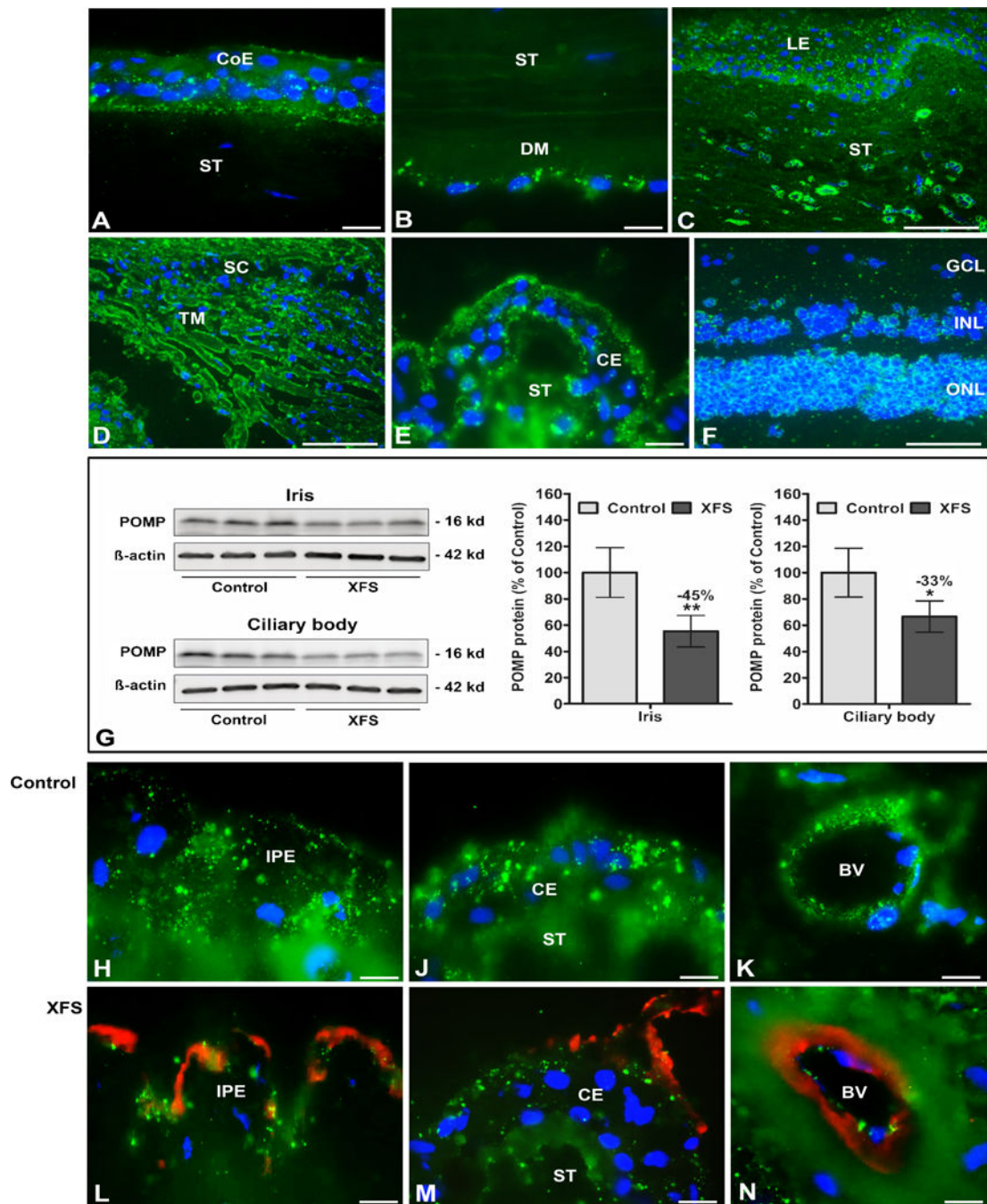


Figure 2.

Manhattan plot of the results from the GWAS discovery plus replication meta-analysis comprising 13,620 XFS cases and 109,837 controls. Genetic markers are plotted according to chromosomal location on the horizontal axis and statistical significance on the vertical axis. SNP markers at seven independent loci surpass genome-wide significance (defined as $P < 5 \times 10^{-8}$). They are *LOXL1*, *CACNA1A*, *POMP*, *TMEM136*, *AGPAT1*, *SEMA6A* and *RBMS3*.

**Figure 3.**

Expression of POMP protein in ocular tissues of normal human donor eyes and donor eyes with XFS, as determined by Western blotting and immunohistochemistry. Immunofluorescence labelling of normal eye tissues shows punctate POMP immunopositivity (green fluorescence) in the cytoplasm of the corneal epithelium (A), the corneal endothelium (B), limbal epithelium and stromal cells (C), trabecular meshwork endothelium (D), ciliary epithelium (E), and retinal cell layers (F).

Reduced POMP protein expression levels in iris and ciliary body tissues of XFS eyes compared to age matched controls are shown by Western blot analysis (G), and by immunofluorescence labelling of iridal (H,L) and ciliary epithelia (J,M) as well as vascular endothelia in the iris (K,N). Reduced staining intensity in XFS tissues is associated with LOXLI-positive exfoliation material accumulations (red immunofluorescence) on the surface of the iris pigment epithelium (L), ciliary epithelium (M) and iris blood vessel walls (N). Western blot (cropped images) and densitometry analysis shows reduced POMP protein expression in iris and ciliary body tissue lysates of XFS eyes compared to control eyes (G). Data are shown as the POMP/B-actin ratio (n=6 for each group; mean \pm standard deviation; *P<0.01; **P<0.005); uncropped versions of all Western blots are shown in Supplementary Figure 16. (BV blood vessel, CE ciliary epithelium, CoE corneal epithelium, DM Descemet membrane, GCL retinal ganglion cell layer, INL inner nuclear layer, IPE iris pigment epithelium, LE limbal epithelium, ONL outer nuclear layer, SC Schlemm's canal, ST stroma, TM trabecular meshwork; DAPI nuclear counterstain in blue; scale bars = 100 μ m in C,D,F and 20 μ m in A,B,E,H-N).

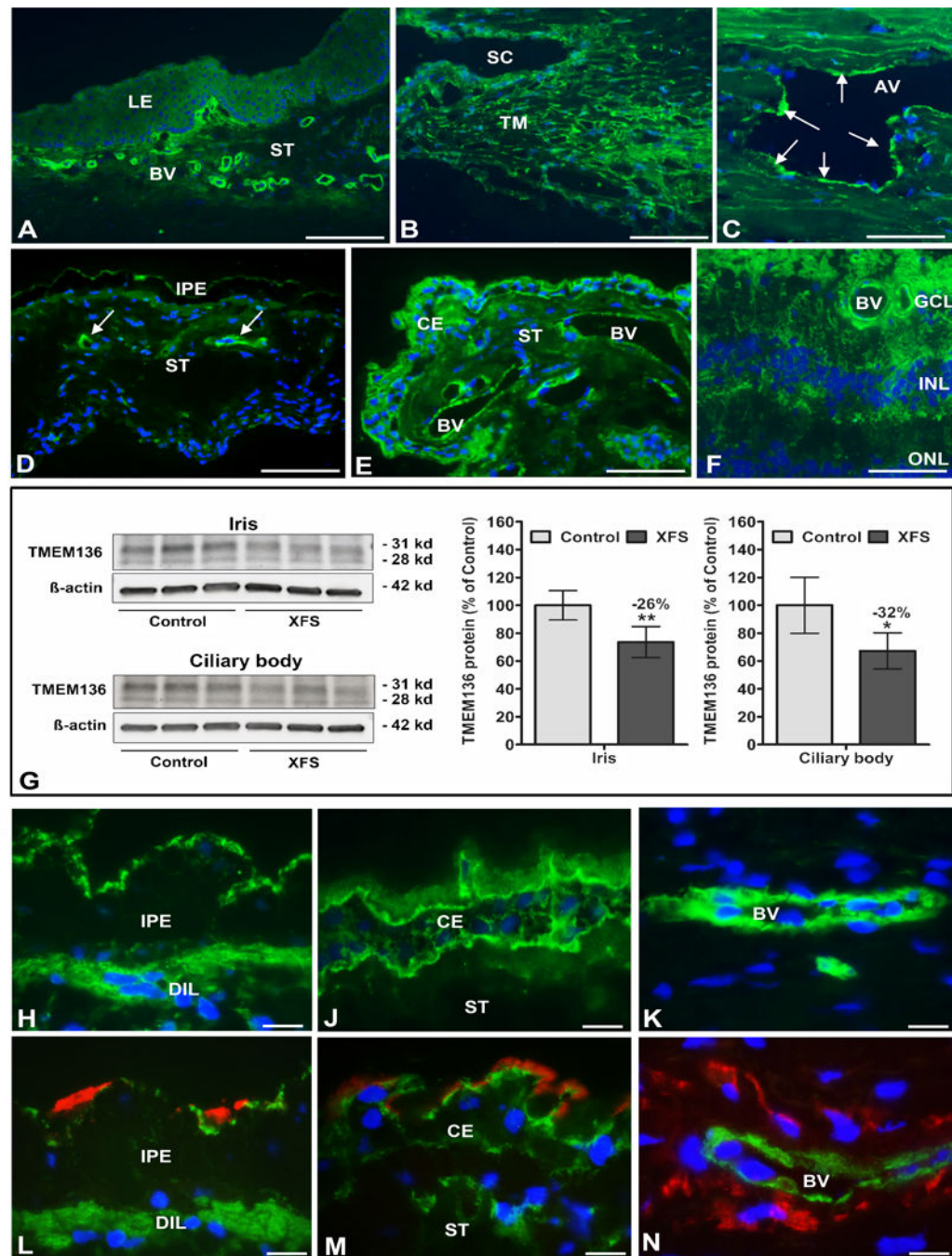


Figure 4.

Expression of TMEM136 protein in ocular tissues of normal human donor eyes and donor eyes with XFS, as determined by Western blotting and immunohistochemistry. Immunofluorescence labelling of normal eye tissues shows cytoplasmic TMEM136 immunopositivity (green fluorescence) in limbal blood vessels (A), trabecular meshwork and Schlemm's canal endothelium (B), walls of aqueous veins (arrows) (C), blood vessels of the iris (arrows) (D), blood vessels and epithelia of the ciliary body (E), and retinal blood vessels and cell layers (F).

Reduced TMEM136 protein expression levels in iris and ciliary body tissues of XFS eyes compared to age matched controls are shown by Western blot analysis (G), and by immunofluorescence labelling of iridal (H,L) and ciliary epithelia (J,M) as well as vascular endothelia in the iris (K,N). Reduced staining intensity in XFS tissues is associated with LOXL1- positive exfoliation material accumulations (red immunofluorescence) on the surface of the iris pigment epithelium (L), ciliary epithelium (M) and iris blood vessel walls (N). Western blot (cropped images) and densitometry analysis shows reduced TMEM136 protein (isoform 1 at 28 KD and isoform 3 at 31 KD) expression in iris and ciliary body tissue lysates of XFS eyes compared to control eyes (G). Data are shown as the TMEM136/B-actin ratio (mean \pm standard deviation; n=6 for each group; * P <0.01; ** P <0.005); uncropped versions of all Western blots are shown in Supplementary Figure 17. (AV aqueous vein, BV blood vessel, CE ciliary epithelium, DIL dilator muscle, GCL retinal ganglion cell layer, INL inner nuclear layer, IPE iris pigment epithelium, LE limbal epithelium, ONL outer nuclear layer, SC Schlemm's canal, ST stroma, TM trabecular meshwork; DAPI nuclear counterstain in blue; scale bars = 200 μ m in A, 100 μ m in B-F and 20 μ m in H-N).

Table 1

Association of all rare, non-synonymous variants at *LOXLI* and risk of exfoliation syndrome. No additional filters by functional effect prediction algorithms were applied. Frequencies for rare variant carriers are given in percentages.

Collection	N cases	N controls	Allele burden cases	Allele burden controls	Carrier freq cases	Carrier freq controls	Allele OR	L95	U95	<i>P</i>
Japanese	2827	3013	34	100	1.20	3.32	0.36	0.24	0.53	8.03×10^{-8}
Greece	355	1075	3	17	0.85	1.58	0.53	0.16	1.82	0.44
Italy	454	267	10	3	2.20	1.12	1.97	0.54	7.19	0.39
Russia	476	859	2	5	0.42	0.58	0.72	0.14	3.72	1
USA	212	161	2	2	0.94	1.24	0.76	0.11	5.41	1
Mexico	116	205	2	9	1.72	4.39	0.39	0.083	1.81	0.34
South Africa	95	250	1	21	1.05	8.40	0.12	0.016	0.90	0.014
India	648	263	12	8	1.85	3.04	0.61	0.25	1.49	0.32
Pakistan	383	186	7	4	1.83	2.15	0.85	0.25	2.92	0.76
Stratified meta-analysis for all sequenced collections							0.46	0.34	0.62	4.2×10^{-7}

Table 2

Association of rare, non-synonymous variants at *LOXLI* and risk of exfoliation syndrome tagged as deleterious by five functional prediction algorithms (SIFT, Polyphen2-HumDiv, LRT score, MutationTaster, and CONDEL). Frequencies for rare variant carriers are given in percentages.

Collection	N cases	N controls	Allele burden cases	Allele burden controls	Carrier freq cases	Carrier freq controls	OR	L95	U95	P
Japanese	2827	3013	11	85	0.39	2.82	0.14	0.073	0.26	3.49×10^{-13}
Greece	355	1075	1	6	0.28	0.56	0.50	0.061	4.19	1
Italy	454	267	1	3	0.22	1.12	0.20	0.020	1.88	0.15
Russia	476	859	0	4	0	0.47	0	N/A	N/A	0.56
USA	212	161	1	1	0.47	0.62	0.76	0.047	12.18	1
Mexico	116	205	0	0	0	0	0	NA	NA	1
South Africa	95	250	0	2	0	0.80	0	NA	NA	0.38
India	648	263	5	7	0.77	2.66	0.29	0.091	0.91	0.047
Pakistan	383	186	0	3	0	1.61	0	NA	NA	0.035
Stratified meta-analysis for all sequenced collections							0.18	0.11	0.30	4.23×10^{-11}
Meta-analysis excluding Russia, Mexico, South Africa, and Pakistan *							0.19	0.11	0.31	1.41×10^{-10}

* Excluding collections where allele zero in either cases or controls

Table 3

Association between *LOXLI* p.Y407F (rs201011613, A>T base change) and exfoliation syndrome.

p.Y407F	N cases	N controls	Allele count in cases (%)	Allele count controls	Freq. cases (%)	Freq. controls (%)	OR	L95	U95	<i>p</i>
Japan sequencing	2827	3013	1	36	0.018	0.60	0.029	0.0040	0.21	8.3×10^{-10}
Japan replication	1082	2325	1	32	0.046	0.69	0.067	0.0091	0.49	8.9×10^{-5}
Japan Combined	3909	5338	2	68	0.026	0.64	0.040	0.0098	0.16	2.9×10^{-14}
European sequencing	1613	2567	0	0	0.0	0.0	-	-	-	-
South Africa sequencing	95	250	0	0	0.0	0.0	-	-	-	-
South Asia sequencing	1031	449	0	0	0.0	0.0	-	-	-	-

This rare variant was found exclusively in the Japanese, and was not polymorphic in Europe, Africa, and South Asia. *P*-values are by Fisher's exact test.

Table 4

Summary of genetic associations for the five newly identified loci.

Chromosome	SNP (effect/ reference)	Position	Gene locus	Stage	Association tests				Heterogeneity tests	
					OR	L95	U95	P-value	P_{het}	I^2 index
13	rs7329408 (A/G)	29166671	<i>FLT1</i> - <i>POMP</i>	GWAS discovery	1.17	1.11	1.22	2.97×10^{-10}	0.9	0.00%
				Replication summary	1.18	1.11	1.25	9.63×10^{-8}	0.17	23.20%
				All data summary	1.17	1.13	1.22	1.56×10^{-16}	0.62	0.00%
				European Caucasian summary //	1.22	1.15	1.29	7.82×10^{-12}		
				Asian summary	1.13	1.07	1.19	1.61×10^{-5}		
11	rs11827818 (G/A)	120198728	<i>TMEM136</i>	GWAS discovery	1.10	1.05	1.16	0.0001	0.10	28.10%
				Replication summary	1.18	1.11	1.25	1.96×10^{-8}	0.36	8.00%
				All data summary	1.14	1.09	1.18	5.86×10^{-11}	0.09	23.10%
				European Caucasian summary //	1.14	1.08	1.20	2.09×10^{-6}		
				Asian summary	1.15	1.08	1.22	4.35×10^{-6}		
6	rs3130283 (A/C)	32138545	<i>AGPAT1</i>	GWAS discovery	1.19	1.11	1.27	1.29×10^{-6}	0.38	5.60%
				Replication summary	1.15	1.07	1.24	0.00013	0.96	0.00%
				All data summary	1.17	1.11	1.23	7.62×10^{-10}	0.81	0.00%
				European Caucasian summary //	1.13	1.06	1.22	0.00034		
				Asian summary	1.24	1.14	1.34	2.27×10^{-7}		
3	rs12490863 (A/G)	29907310	<i>RBMS3</i>	GWAS discovery	1.15	1.09	1.22	4.9×10^{-7}	0.69	0.00%
				Replication summary	1.12	1.04	1.20	0.002	0.13	26.50%
				All data summary	1.14	1.09	1.19	7×10^{-9}	0.23	12.50%
				European Caucasian summary //	1.19	1.11	1.27	1.64×10^{-6}		
				Asian summary	1.12	1.05	1.20	0.00053		
5	rs10072088 (G/A)	116019417	<i>SEMA6A</i>	GWAS discovery	0.89	0.85	0.94	2.3×10^{-5}	0.85	0.00%
				Replication summary	0.88	0.83	0.94	0.00017	0.10	36%
				All data summary	0.89	0.85	0.93	1.5×10^{-8}	0.66	0.00%

					Association tests			Heterogeneity tests	
Chromosome	SNP (effect/ reference)	Position	Gene locus	Stage	OR	L95	U95	P-value	<i>P</i> _{het} I ² index
				European Caucasian summary //	0.90	0.85	0.94	2.83 × 10 ⁻⁵	
				Asian summary	0.88	0.81	0.96	0.0024	

// This summary includes 7,113 cases and 95,863 controls from North America, Northern-, Southern-, Eastern-, and CentralWestern Europe. This summary does not include Latin and South America.

Author Manuscript

Author Manuscript

Author Manuscript

Author Manuscript